UNIVERSITY OF CALIFORNIA, SAN DIEGO
SCRIPPS INSTITUTION OF OCEANOGRAPHY
VISIBILITY LABORATORY
SAN DIEGO, CALIFORNIA 92152

COMPUTER ANALYSIS AND SIMULATION OF UNDERWATER CAMERA SYSTEM PERFORMANCE

B. L. McGlamery

SIO Ref. 75-2
January 1975

Naval Supply Center
Code 87, Bldg. 442E
Oakland, California 94625

Approved:

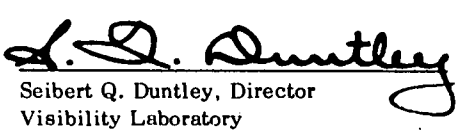

Seibert Q. Duntley, Director
Visibility Laboratory

Approved for Distribution:

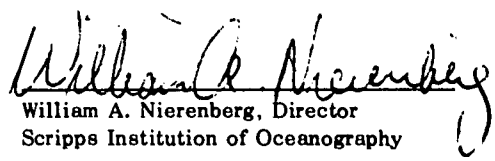

William A. Nierenberg, Director
Scripps Institution of Oceanography

UNCLASSIFIED

SECURITY CLASSIFICATION OF THIS PAGE *(When Data Entered)*

REPORT DOCUMENTATION PAGE		READ INSTRUCTIONS BEFORE COMPLETING FORM
1. REPORT NUMBER SIO Ref. 75-2	2. GOVT ACCESSION NO.	3. RECIPIENT'S CATALOG NUMBER
4. TITLE *(and Subtitle)* COMPUTER ANALYSIS AND SIMULATION OF UNDERWATER CAMERA SYSTEM PERFORMANCE		5. TYPE OF REPORT & PERIOD COVERED Final Report – Task 4 1 September to 31 August 1974 6. PERFORMING ORG. REPORT NUMBER
7. AUTHOR(s) B. L. McGlamery		8. CONTRACT OR GRANT NUMBER(s) N66314-74-C-8016
9. PERFORMING ORGANIZATION NAME AND ADDRESS Visibility Laboratory, University of California, San Diego Scripps Institution of Oceanography San Diego, California 92152		10. PROGRAM ELEMENT, PROJECT, TASK AREA & WORK UNIT NUMBERS Task 4
11. CONTROLLING OFFICE NAME AND ADDRESS Naval Supply Center Code 87, Bldg. 442E Oakland, California 94625		12. REPORT DATE June 1975 13. NUMBER OF PAGES 53
14. MONITORING AGENCY NAME & ADDRESS*(if different from Controlling Office)*		15. SECURITY CLASS. *(of this report)* UNCLASSIFIED 15a. DECLASSIFICATION/DOWNGRADING SCHEDULE

16. DISTRIBUTION STATEMENT *(of this Report)*

Approved for public release; distribution unlimited.

17. DISTRIBUTION STATEMENT *(of the abstract entered in Block 20, if different from Report)*

18. SUPPLEMENTARY NOTES

19. KEY WORDS *(Continue on reverse side if necessary and identify by block number)*

Underwater Optics

Computer Simulation

20. ABSTRACT *(Continue on reverse side if necessary and identify by block number)*

This report presents the development of a numerical method for computer analysis of underwater camera systems.

The approach uses fundamental measurable water properties such as the volume scattering function, the beam spread function, and the optical transfer function, to calculate all of the lighting components that exist in the film plane of any submerged camera. The technique can

DD FORM 1 JAN 73 1473 EDITION OF 1 NOV 65 IS OBSOLETE
S/N 0102-014-6601

UNCLASSIFIED

SECURITY CLASSIFICATION OF THIS PAGE *(When Data Entered)*

Block 20 (Cont)

be used to simulate the performance of any combination of lights, camera, type of water, object, and object to camera distance. It can be used to produce accurate computer generated pictures of submerged objects including modeling of sensor noise, lens effects, etc.

Included in the report are examples of calculations of the image plane light components as a function of source-object-camera geometry, computer simulated high resolution images of a submerged object and enhanced versions of the simulated image to demonstrate the utility of post detection image processing. The enhancement techniques include a constant variance enhancement filter which allows low contrast detail to be extracted from a scene with widely varying light levels.

SUMMARY

The analysis of the performance of underwater camera systems is greatly complicated by the absorption and scattering of light in the water between the camera and the object. This report presents a computer based numerical approach to the solution of the problem.

The approach consists of computing all of the lighting components that exist in the sensor image plane of a submerged camera using as input parameters the geometry of the camera system and fundamental measured optical properties of the water. The image plane light components which are calculated are the direct image formed by non-scattered light from the object, the glow-field image formed by scattered light from the object, and the backscatter image formed by light from the source scattered towards the camera. These images are evaluated for the full field of view of the camera. The fundamental water properties used in the calculation are the volume scattering function, the beam spread function, and the point spread function. Equations are developed which relate the three image components to these water properties. Evaluation of the equations is done by a digital computer using array processing.

Applications of the basic method of calculation are discussed. One application is analysis of system performance as a function of the source, object and camera locations, and the beam pattern of the source. This application allows the system designer to optimize the system design by considering tradeoffs between system geometry, source distribution and power, image contrast, and image signal-to-noise ratio. Sample calculations are shown. A second application consists of the computer generation of high resolution photographs which simulate the appearance of an object as it would appear when imaged by a specific camera system with a specific set of water properties. An example of this application is shown. Included in this example are computer enhanced pictures of the image that would be formed in the image plane. The enhancement includes simple contrast enhancement and a more sophisticated method of constant variance enhancement which allows low contrast detail to be extracted from a scene with widely varying light levels.

TABLE OF CONTENTS

LIST OF ILLUSTRATIONS

1. INTRODUCTION

The quality of the image formed by an underwater camera system is often profoundly affected by the optical properties of the water medium between the source, object, and camera. The absorption and scattering of light by the water may significantly limit the useful range and resolution of the camera.

Conceptually, the effect of the scattering and absorption by the water on the image is easy to visualize. Light from the source irradiates the object with both scattered and non-scattered light. Light reflected from the object is absorbed or transmitted by the water. Some of the transmitted reflected light reaches the camera without scattering and produces a direct image component of high quality. Some of the transmitted reflected light reaches the camera via scattering processes and results in a blurred image with little structure. In addition, light from the source scattered by the water back towards the camera is imaged by the camera, resulting in a reduction of contrast of the above image components.

Actual numerical analysis of the camera image formed as described, however, is quite laborious. The source beam spreads beyond its intrinsic shape with increasing distance from the source due to scattering. This beam spread, combined with attenuation of the beam, can lead to non-uniform illumination of the object. Light reflected from a point on the object does not image as a point, but as an extended point spread function. Because of absorption and scattering, the total power in the point spread function and its distribution in the image plane is a function of the distance between the camera and the point on the object. The net result is that the image plane component due to reflected light from the object consists of the convolution of a shift-variant point spread function with a non-uniformly illuminated object. Analysis of the light from the source scattered back towards the camera and imaged is even more complicated. The contribution of an elemental scattering volume to the image in the camera depends on a variety of factors related to the position of the volume with respect to the source and camera and to the scattering and absorption properties of the water. Calculation of the final image is thus a formidable undertaking if all of the effects are considered.

Fortunately the required calculations are within the capability of present day computers if appropriate simulation methods are used. This report deals with such a method that has been developed and implemented at the Visibility Laboratory. In this report the mathematical formulation of the method will be developed and examples of computer implementation of the model will be presented.

The simulation method is primarily for the case in which the object to be viewed is irradiated by a single source of narrow optical bandwidth incoherent light. Analysis of systems with more than one source or broad bandwidth can be accomplished by combining the results of the analyses for separate sources and wavelengths.

The simulation technique is based upon the use of observable macroscopic optical properties of water such as the volume attenuation coefficient[1], volume scattering function[1], the beam spread function[2], and the point spread function (spatial impulse response function)[3].

The volume scattering function is important in the calculation of backscattered light. This function describes the distribution of scattered light around an elemental scattering volume. Its use in the simulation model consists mostly of a table look-up of the value of the function in those calculations where it is needed.

The beam spread function is a very important part of the simulation method. The beam spread function describes the spreading of a very thin beam in water. Convolution in angular coordinates of this function with the intrinsic beam pattern of a source produces the beam pattern that is obtained in water with scattering. Analytic equations which fit empirical beam spread data have been developed by Dr. Wayne Wilson of the Visibility Laboratory.[4] In addition Wilson has developed a computer program which performs the angular convolution of the beam spread function with an intrinsic source distribution so that the irradiance in any point in space around a source can be computed. This ability is a key element in the model presented here. Description of the analytical beam spread equations and the convolution process will be made in a separate report by Wilson. In the present report the assumption will be made that the irradiance on a surface at any location in the water due to a known source is an available quantity.

Of equal importance to the simulation method is the means of representing the point spread function of water. The point spread function is a representation of the image of a point source object. Its Fourier transform is the optical transfer function.[5] Its characteristics are a function of water properties and the distance between the camera and object. The point spread function representation used in the present model is based on measurements made on the image of a point source object in a tank of sea water. The analytical representation of the point spread function based on these measurements was developed by James L. Harris, Sr.. The representation is a good one over the range of distances for which the measurements were made and for the water used. The extension of the representation to other distances and waters is presently being investigated. The results will be presented in a future report by Wilson.

2. COORDINATE SYSTEM AND DEFINITIONS

Figure 1 depicts the general imaging problem. A source at an arbitrary location irradiates an object, which is viewed by a camera at an arbitrary location. Four coordinate systems are required to conveniently represent this problem numerically. These coordinate systems, depicted in Figure 1, are:

(1) A general space coordinate system, (x_o, y_o, z_o) which is used to specify the object reflectance map, the source, and the camera locations.

(2) A source coordinate system, (x_s, y_s, z_s), in which the optical axis of the source lies along the z_s axis. This system is convenient for determination of source irradiance at a point in space with respect to the source.

(3) A camera coordinate system, (x_c, y_c, z_c), in which the optical axis of the camera lies along the z_c axis. This system is useful for computing distances from the camera to points in object apace and angles between these points and the camera axis.

(4) An image plane coordinate system (x_i, y_i) which is used for describing the irradiance components in the camera image plane. It is a two-dimensional system with the x_i and y_i axis lying in the image plane. The image plane x_i and y_i coordinates are related to the camera x_c and y_c coordinates by a multiplicative constant.

In the computer method which has been developed all of these coordinates systems are used. However, in the development here inclusion of all of the coordinate systems would greatly complicate notation while adding little information. Therefore, only two coordinate systems will be used in the development. The source coordinate system is omitted by assuming that source irradiance is expressed as a function of the space coordinates rather than the source coordinates, implying that the correct coordinate transformation has already been done. This is appropriate since, as explained in the introductory section, the mechanics of computing the source irradiance will not be treated in this report. The camera coordinate system will also be eliminated by placing the camera on the z axis of the space coordinate system so that points in space with respect to the camera can easily be represented in the space coordinate system. Thus the two remaining coordinate systems are the space coordinate system and the image plane coordinate system. These are shown in Figure 2. The space coordinates are denoted by (x',y',z'). The image plane coordinates are denoted by (x,y). The (x,y) plane is parallel to the (x',y') plane. The camera is located a height of Z_c above the (x',y') plane. Note the sign reversal of the (x,y) coordinates to account for the inversion of the lens.

Using this simplified coordinate system, expressions for the various irradiance components in the image plane will now be developed.

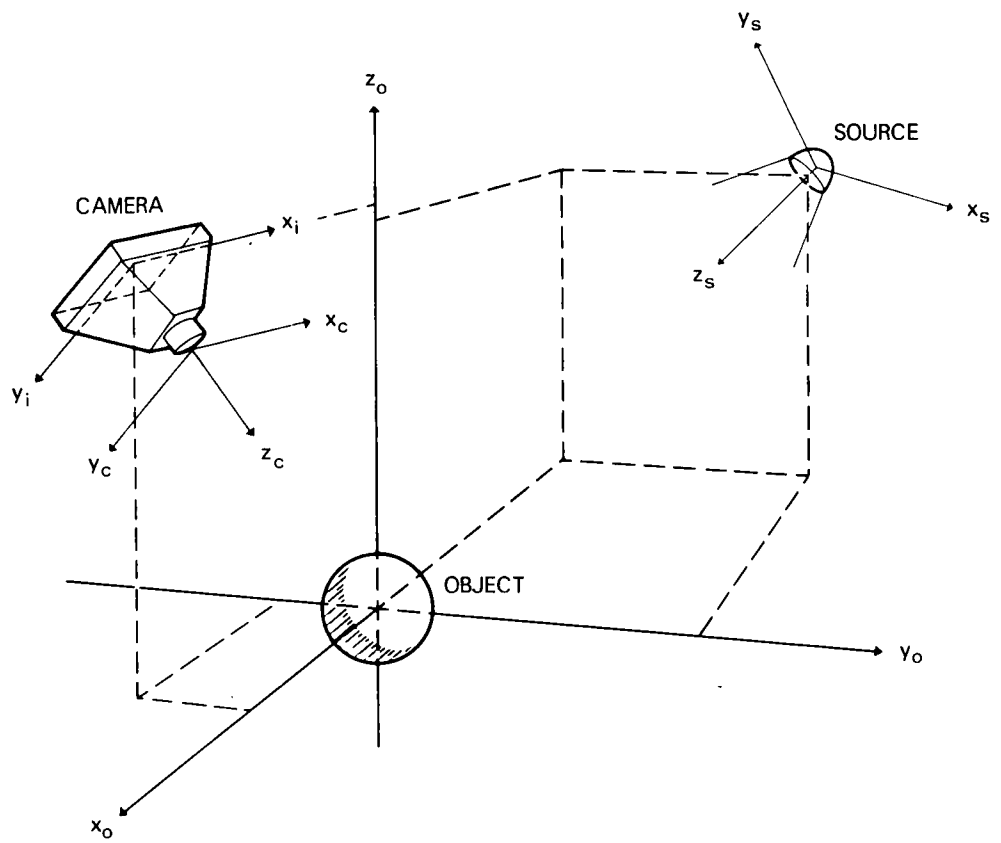

Fig. 1. Coordinates for a generalized underwater optical system.

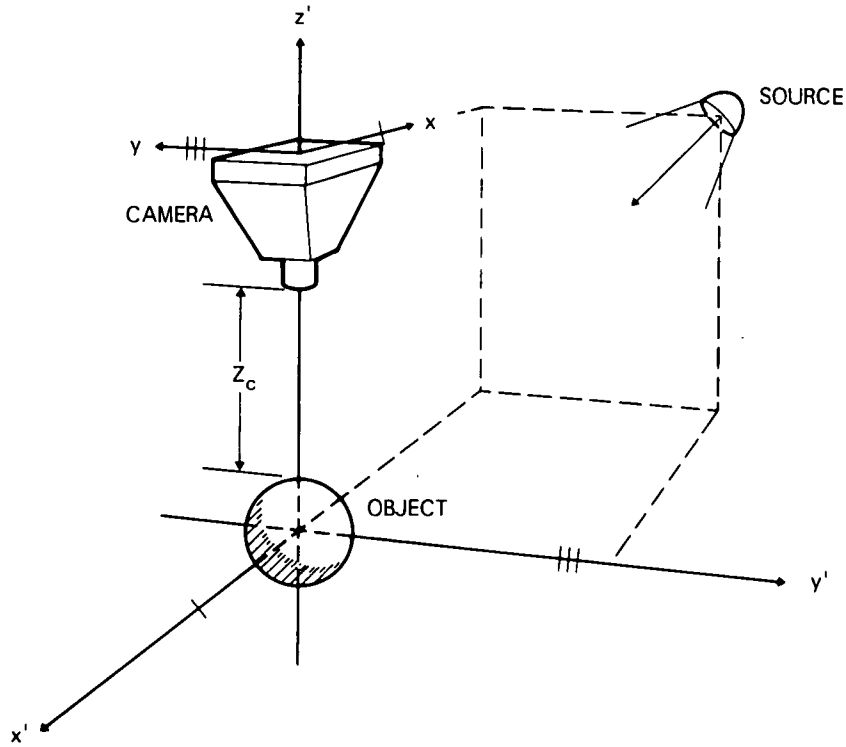

Fig. 2. Simplified coordinates for concept development.

3. DEVELOPMENT OF THE METHOD

3.1 IRRADIANCE COMPONENTS DUE TO REFLECTED LIGHT

IMAGE PLANE IRRADIANCE

The first step will be to develop the equations for the irradiance distribution in the image plane due to light reflected from the object. We initially assume a two-dimensional object which is in the $z' = 0$ plane. An approximate method by which a three-dimensional object can be treated will be discussed in Section 3.4. Let the object be represented by an equivalent two-dimensional reflectance map, $R(x',y',0)$. Consider an elemental area on the object, as shown in Figure 3. The image plane irradiance at (x,y) due to an element of area at (x',y') will be calculated. The relationships between x and x' and y and y' are

$$\begin{aligned} x &= mx' \\ y &= my' \end{aligned} \tag{1}$$

where m is the magnification of the system given by

$$m = l/Z_c \ . \tag{2}$$

Z_c is the distance between the camera and the $x'-y'$ plane and l is the image plane distance given by

$$l = \frac{F_\ell \, Z_c}{Z_c - F_\ell} \ , \tag{3}$$

where F_ℓ is the focal length of the optical system.

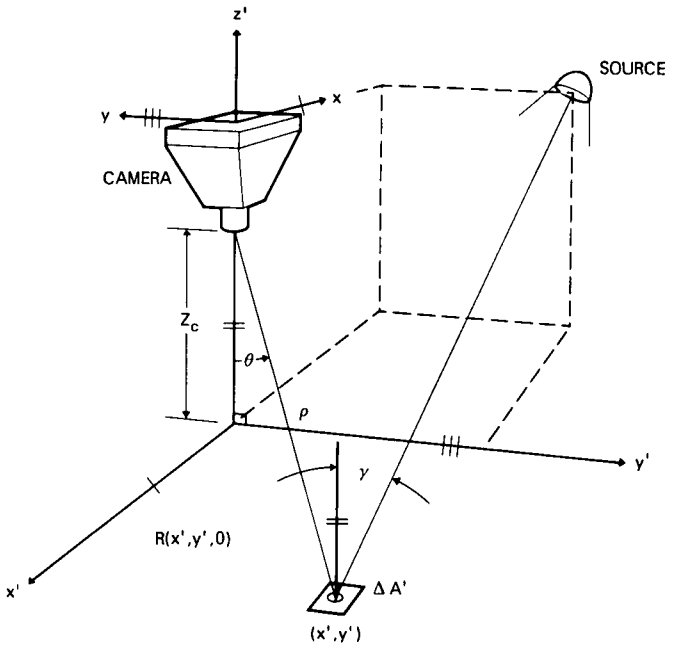

Fig. 3. Geometry for calculating image plane irradiance due to object.

The source irradiance at $(x',y',0)$ on an area perpendicular to the radius vector from the source is $H_s(x',y',0)$. The irradiance on an area in the $x'-y'$ plane is $H_s(x',y',0)\cos\gamma(x',y',0)$ where $\gamma(x',y',0)$ is the angle between the perpendicular to the elemental area and the source. This is an approximation because the flux at $(x',y',0)$ is not coming directly from the source but, due to scattering of the light between the source and the object, arrives at $(x',y',0)$ from a distribution of angles. Therefore, the irradiance on a surface would not vary exactly as $\cos\gamma$. While the magnitude of this error has not been evaluated for actual angular distributions, a calculation with a simple distribution has shown the error to be small.

At this point the development proceeds as if the reflected light from the object plane is received by the camera without any absorption or scattering effects. These effects will be included later (see page 3-4). The radiance of a Lambertian reflector with reflectance R and irradiance H is given by

$$N = \frac{HR}{\pi}\left(\frac{\text{watts}}{\text{m}^2 - \text{steradian}}\right) . \tag{4}$$

Thus the radiance due to the object at $(x',y',0)$ is

$$N(x',y,0) = \frac{H_s(x',y',0)\,R(x',y',0)\cos\gamma(x,y,0)}{\pi} . \tag{5}$$

The power, $P_i(x',y',0)$, received from the elemental area $\Delta A'$ at $(x',y',0)$ and transmitted by a lens having a diameter D and a transmittance of T_ℓ is

$$P_i(x',y'0) = N(x',y',0)\,\Delta A'\,\cos\theta(x',y',0)\,\Omega_\ell(x',y',0)\,T_\ell \quad , \tag{6}$$

where θ is the nadir angle as shown in Figure 3, and $\Delta A'\cos\theta$ is the projected area of the elemental area. The solid angle subtended by the lens Ω_ℓ is given by

$$\Omega_\ell(x',y',0) = \frac{\pi D^2\cos\theta(x',y',0)}{4\rho^2(x',y',0)} \tag{7}$$

where ρ is the distance from the camera to the $(x',y',0)$ point, as shown in Figure 3. The $\cos\theta$ factor accounts for the reduction of the effective area of the lens for off-axis points. Thus using Eqs. (5) and (7) in Eq. (6) gives

$$P_i(x',y',0) = \frac{H_s(x',y',0)\,R(x',y',0)\,\Delta A'\,D^2\cos^2\theta(x',y',0)\cos\gamma(x',y',0)\,T_\ell}{4\rho^2(x',y',0)} \quad . \tag{8}$$

Assuming a distortionless lens this power is imaged into an area in the image plane of $m^2\Delta A'$. Thus the image plane irradiance $H_i(x,y)$ is given by

$$H_i(x,y) = \frac{P_i(x',y',0)}{m^2\Delta A'} \quad . \tag{9}$$

Using Eqs. (2) and (3) for m, Eq. (9) becomes

$$H_i(x,y) = \frac{P_i(x',y',0)\,(Z_c - F_\ell)^2}{F_\ell^2\,\Delta A'} \quad . \tag{10}$$

If Eq. (8) is used for P_1 in Eq. (10) and if the following substitutions are made

$$\rho^2(x',y',0) = \frac{Z_c^2}{\cos^2\theta(x',y',0)} , \tag{11}$$

$$(f\#)^2 = F_\ell^2/D^2 , \tag{12}$$

where f# is the f number of the optical system, then $H_1(x,y)$ becomes

$$H_1(x,y) = \frac{H_s(x',y',0)\, R(x',y',0) \cos^4\theta(x',y',0) \cos\gamma(x',y',0)\, T_\ell}{4f\#^2} \cdot \left(\frac{Z_c - F_\ell}{Z_c}\right)^2 . \tag{13}$$

THE POINT SPREAD FUNCTION

Up to now the derivation has neglected the scattering and absorption by the water on the light reflected by the object. The assumption has been that an element of area at the point (x_p',y_p') will image only at (x_p,y_p), where p denotes a dummy variable. The power associated with this element of area is

$$H_1(x_p,y_p)\, dx_p\, dy_p \text{ (watts)} . \tag{14}$$

In the presence of scattering and absorption this power will be redistributed in the image plane according to the point spread function $S[(x,y);(x_p',y_p',z_p')]$. The point spread function gives the image plane irradiance over the x−y plane due to a point in object space located at (x_p',y_p',z_p') which in the absence of scattering and absorption would image at (x_p,y_p). Another way of denoting the dependence of S on the location of the point in object space is to use the image plane coordinates (x_p,y_p) so that $S = S[(x,y); (x_p,y_p), z_p']$. This notation will be convenient later on. The units of S are watts/m²/watt input power, or $1/m^2$. Thus multiplying S by Eq. (14) gives the irradiance in the image plane due to a single elemental area on the object at (x_p',y_p',z_p'). Integrating this product over the entire image plane distribution gives the image plane irradiance with scattering and absorption effects included, $H_2(x,y)$. It is expressed by

$$H_2(x,y) = \iint H_1(x_p,y_p)\, S[(x,y);(x_p,y_p), z_p']\, dx_p\, dy_p . \tag{15}$$

The expression for H_2 in Eq. (17) is a convolution integral. For computational ease one would like to compute H_2 by means of Fourier transform techniques. Such techniques would require S to be shift invariant, i.e., S would not change in shape or magnitude as a function of x_p or y_p. In general S is not shift invariant, for several reasons. The distance between the receiver and points on the object plane is $\rho = (x_p'^2 + y_p'^2 + z_p'^2)^{1/2}$. Thus the further off-axis an elemental area is, the greater is the distance to the receiver, leading to greater absorption and scattering. (Note that inverse square falloff for off-axis points is already built into Eq. (15) in terms of a $\cos^2\theta$ component). The greater absorption decreases the total energy in the point spread function while the greater scattering results in a larger size of the point spread function for off-axis points.

As an example of the decrease in magnitude of the total energy due to absorption for off-axis points, assume that the total flux from a point source imaged by the camera is approximately proportional to $(e^{-G\rho})\rho^2$ where G is an attenuation coefficient. The $1/\rho^2$ dependence has already been accounted for in the derivation of the image plane irradiance (see Eq. 11). Now $\rho = Z_c/\cos\theta$. Thus the ratio of attenuation of an off-axis point to an on-axis point (neglecting the $1/\rho^2$ dependence) is

$$\frac{e^{-GZ_c/\cos\theta}}{e^{-GZ_c}} = e^{-GZ_c(1/\cos\theta - 1)} . \tag{16}$$

This quantity is tabulated in Table I with GZ_c expressed in attenuation lengths.

Table I

	$e^{-GZ_c(1/\cos\theta - 1)}$				
	GZ_c, attenuation lengths				
θ	2	4	6	8	10
0	1.0	1.0	1.0	1.0	1.0
10	.97	.94	.91	.885	.85
20	.880	.773	.680	.598	.526
30	.734	.539	.395	.290	.213
40	.543	.294	.160	.0869	.0472
50	.328	.108	.0354	.0116	3.81×10^{-3}
60	.135	.0183	2.49×10^{-3}	3.35×10^{-4}	4.54×10^{-5}

Even for moderate conditions such as $\theta = 30°$ and an on-axis distance of 4 attenuation lengths, the off-axis image plane irradiance is down by a factor of $1/.539 = 1.85$.

In addition to off-axis attenuation, a distortion of the point spread function occurs off-axis in the image plane. Due to scattering and absorption, light from a point which would normally enter the lens from a single angle θ now enters the lens over a distribution of angles about θ. The projection of the distribution of these angles onto the image plane is the point spread function. Since the projection is onto a flat plane the width of the projected point spread function depends on θ, as illustrated in Figure 4. Here it can be seen that a bundle of rays $\Delta\theta$ wide projects onto the image plane on-axis as a circle with a diameter of $l\Delta\theta$, where l is the image plane distance. However, off-axis at an angle of θ the same bundle of rays $\Delta\theta$ wide projects onto the image plane as an ellipse with a major axis of $l\Delta\theta/\cos^2\theta$. Thus the ratio of the off-axis diameter to the on-axis diameter is $1/\cos^2\theta$. This elongation factor is tabulated in Table II. Here it can be seen that for points very far off-axis the elongation effect can be quite large.

Table II

Elongation Factor

θ	$1/\cos^2\theta$
0	1.00
10	1.03
20	1.13
30	1.33
40	1.70
50	2.42
60	4.00

To summarize, the point spread function varies off-axis due to

(a) Increased attenuation due to increased distance.

(b) Increased spread due to increased distance.

(c) Distortion of the projection of PSF in image plane.

Thus to handle the convolution of the point spread function with the object reflectance map is computationally very difficult. However, acceptable approximations can be made which will allow useful results to be obtained. These approximations will now be developed.

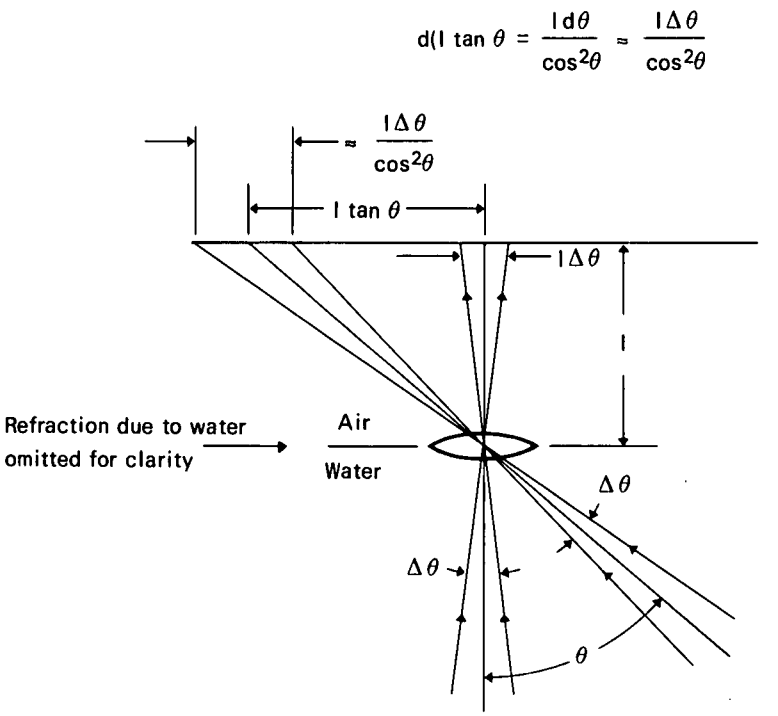

Fig. 4. Off-axis elongation of a point spread function $\Delta\theta$ in width.

In order to introduce the approximate method let us initially assume that the point spread function is shift invariant, i.e., the shape of the point spread function is invariant as its center is moved about the image plane. Then the functional relationship of S on the location of the center of the point spread function (x_p,y_p) and the general image plane coordinates (x,y) can be expressed in terms of the difference coordinates $(x - x_p, y - y_p)$. The convolution integral can then be expressed as

$$H_2(x,y) = \iint H_1(x_p,y_p)\, S[(x-x_p),(y-y_p),z_p']\, dx_p\, dy_p = H_1(x,y) * S(x,y,z') \quad . \tag{17}$$

This convolution can be performed by Fourier techniques. We define the Fourier transform, $\tilde{F}(f_x,f_y)$, of a function $F(x,y)$ as

$$\tilde{F}(f_x,f_y) = \frac{1}{\sqrt{2\pi}} \iint F(x,y)\, e^{-i2\pi (f_x x + f_y y)}\, dx\, dy \quad , \tag{18}$$

and the inverse transform by

$$F(x,y) = \frac{1}{\sqrt{2\pi}} \iint \tilde{F}(f_x,f_y)\, e^{i2\pi(f_x x + f_y y)}\, df_x\, df_y \quad . \tag{19}$$

The variables f_x and f_y are the frequencies of two dimensional spatial sinusoidal functions in the x and y directions. By the convolution theorem[6] the Fourier transform of Eq. (17) can be expressed as a simple frequency by frequency product:

$$\tilde{H}_2(f_x,f_y) = \tilde{H}_1(f_x,f_y) \cdot \tilde{S}(f_x,f_y,z'_\rho) \ , \tag{20}$$

and $H_2(x,y)$ is obtained by taking the inverse transform of Eq. (20). The Fourier transform $\tilde{S}$ of the point spread function is the optical transfer function associated with the water and optical system. It expresses the attenuation and phase shift of spatial sinusoids as a function of their frequency.

In order to proceed beyond this point it is necessary to assume some form for $\tilde{S}$. On the basis of point spread function measurements made in an experimental tank filled with sea water at the Visibility Laboratory, the following form has been adopted as an initial representation of the incoherent optical transfer function for sea water.

$$\tilde{S}(f_\theta) = (e^{-GZ_c} - e^{-\alpha Z_c})\, e^{-BZ_c f\theta} + e^{-\alpha Z_c} \ , \tag{21}$$

where

G = an attenuation coefficient associated with light from a point source.

α = the volume attenuation coefficient. (Alpha)

B = an empirical coefficient related to scattering and the spread of the point spread function.

f_θ = angular spatial frequency, cycles/radian.

Z_c = distance between point of object and camera.

This optical transfer function describes the attenuation of angular spatial frequencies in the image of a point source at a distance Z_c from the camera. Since it is a function of only one frequency variable it corresponds to a radially symmetrical point spread function when on the optical axis of the camera. This optical transfer function neglects any diffraction effects due to the lens, as will be discussed below.

At this point it is appropriate to discuss the concept of spatial angular frequency. The optical transfer function is associated via the Fourier transform with a point spread function. For water the point spread function must be expressed in terms of angular coordinates because it is due to angular deviations of light as it propagates through the water. For a given distance and water properties, light from a point source arrives from a distribution of angles. This distribution of angles can be characterized by $\Delta\theta$, where $\Delta\theta$ might represent the diameter containing 50 percent of the energy or be twice the second moment of the distribution or some other measure. However, when the point spread function is projected on-axis onto a camera image plane it becomes a linear quantity with the dimensions of $2I \sin \Delta\theta/2$, where I is the image distance. For $\Delta\theta$ sufficiently small, say $\Delta\theta < 60°$; $2I \sin(\Delta\theta/2) \approx I\Delta\theta$ (4.7% error). We

now Fourier transform the projected image to obtain the optical transfer function. The optical transfer function gives the amplitude and phases of the linear spatial sinusoids which when added together will give the point spread function. These spatial sinusoids are mathematical abstractions. Any given spatial frequency extends in image space from $-\infty$ to $+\infty$. However, when all sinusoids are added together they reproduce the spatially limited function. If we take a single linear spatial sinusoid in the image plane and try to project it back into angular space, we quickly run into difficulties. This is illustrated in Figure 5. Equal periods of a linear frequency do not project into angular space with equal angular periods. However, it is not necessary to visualize the angular spatial frequencies beyond the angular extent of the point spread function. If we restrict the concept of angular spatial frequencies to the region of the point spread function and if the small angle approximation stated above is satisfied, then the relationship between the image plane linear frequencies, f(cycles/meter) and the angular spatial frequencies f_θ(cycles/rad) is

$$f_\theta = f\,l = (f_x^2 + f_y^2)^{1/2}\,l \quad , \tag{22}$$

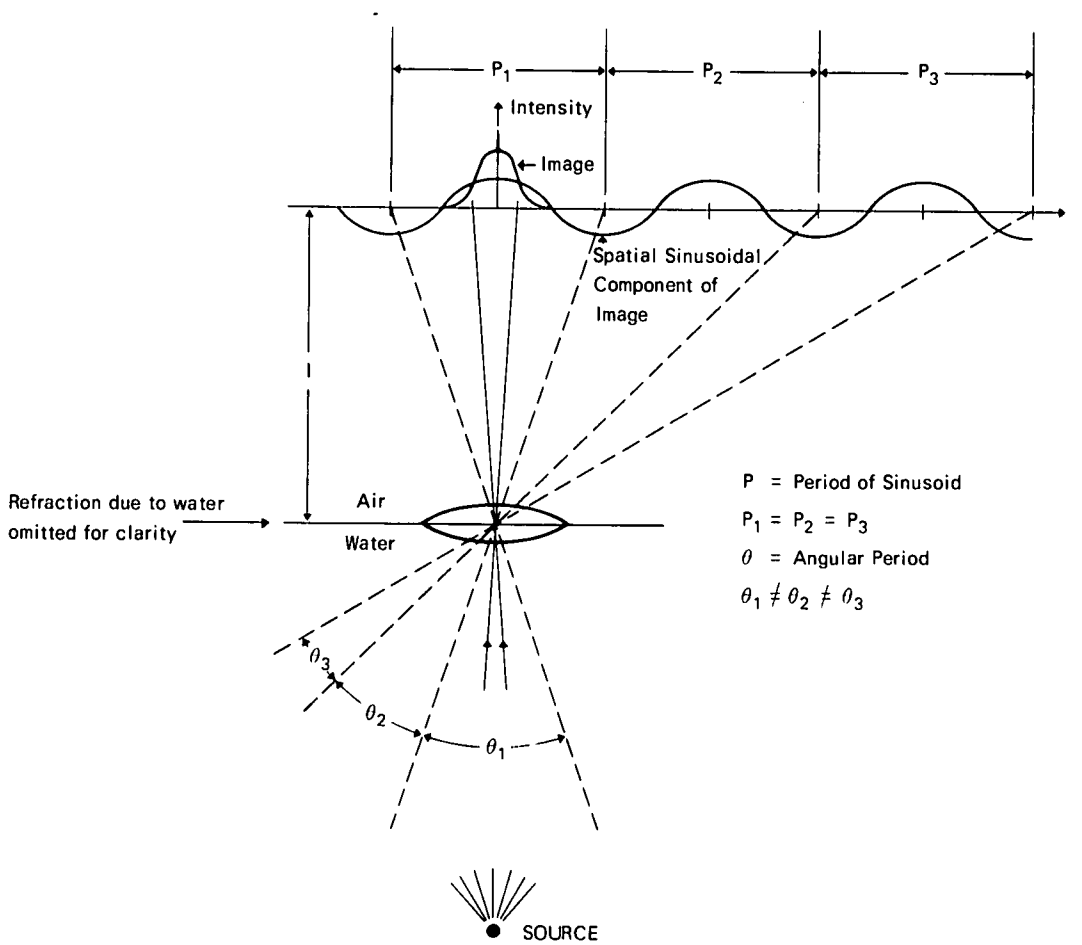

Fig. 5. Projection of linear spatial frequencies into angular space.

where l is the image plane distance given by Eq. (3).

In accordance with the above discussion, Eq. (21) can be written as

$$\tilde{S}(f_x,f_y) = (e^{-GZ_c} - e^{-\alpha Z_c})\, e^{-BZ_c f l} + e^{-\alpha Z_c} \quad . \tag{23}$$

This form for the optical transfer function consists of two distinct components and its associated point spread function also consists of two distinct components. One component represents light propagated between the point source and the camera without having been scattered. This light is imaged by the camera as a point whose total power attenuates as a function of Z_c according to $e^{-\alpha Z_c}$. The Fourier transform of this image component is a constant for all frequencies and has the value of $e^{-\alpha Z_c}$. Note that diffraction is being neglected here since in reality the non-scattered light would actually form a diffraction pattern (the Airy disk) and the Fourier transform would be a decreasing function going to zero at a frequency of $1/(\lambda f\#)$ where $f\#$ is the f number of the lens. Omission of the effects of diffraction implies that the model is intended for use only at spatial frequencies well below the diffraction cutoff of the lens. The reason for this is as follows.

The experiment which provided the data for the model consisted of imaging a point source of light submerged in sea water with a lens a distance Z_c away. Measurements were made for Z_c varying from 3 to 17 $1/\alpha$ distances or attenuation lengths. The pattern observed in the image plane of the lens consisted of a pattern smoothly decreasing from the center of the image with what appeared to be a classical Airy diffraction pattern superimposed on the much larger pattern. This result was found even with lens diameters up to 100mm. The diffraction pattern represented the image formed by nonscattered light from the point source. The fact that a circularly symmetric diffraction pattern did exist indicated that this component of the point spread function was approximately diffraction limited. However, no measurements were made on the shape of the pattern, so small deviations, which could cause the optical transfer function to deviate from the classical function, may have been present. Therefore, to be conservative, we choose to limit the range of applicability of Eqs. (21) and (23) to those regions where the diffraction optical transfer function is high.

The other component of the optical transfer function and the point spread function is due to light from the point source which is propagated to the camera via scattering processes. In the optical transfer function this is the component having an amplitude of $(e^{-GZ_c} - e^{-\alpha Z_c})$ at zero frequency and at higher frequencies the same value attenuated exponentially with frequency according to $e^{-BZ_c f l}$. In the point spread function it is the component having a total power proportional to $(e^{-GZ_c} - e^{-\alpha Z_c})$ distributed in a function which is the inverse Fourier transform of $e^{-BZ_c f l}$. Due to the sometimes broad spread of this component of the point spread function, convolution with an object map produces a blurred glow-like appearance. Thus this component is designated as the glow-field component.

The direct image, glow-field, and total components of the optical transfer function and point spread function are illustrated in Figure 6.

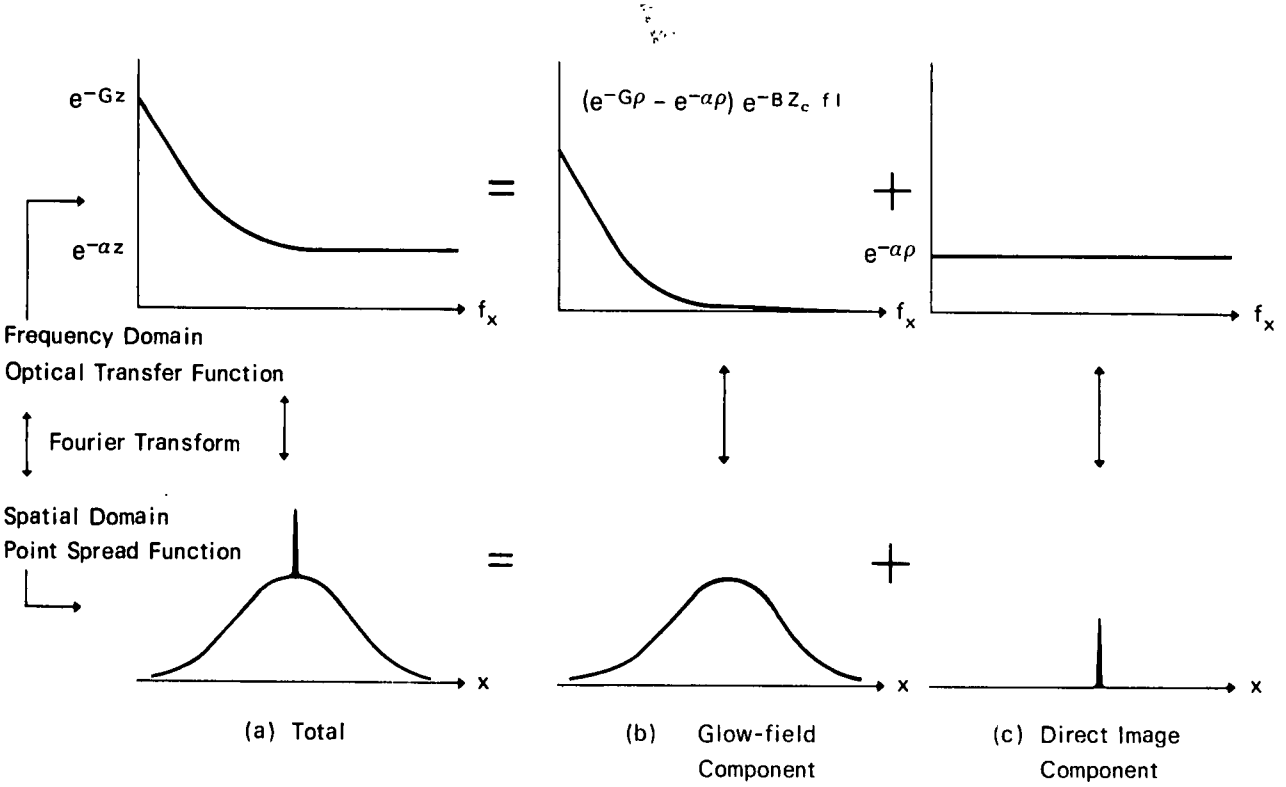

Fig. 6. The glow-field and direct image components of the optical transfer function (top row of figures) and the point spread function (bottom row of figures).

APPLICATION OF THE POINT SPREAD FUNCTION

Let us now express Eq. (23) in terms of the two components described above. Let $\tilde{S}_d$ be the direct component due to nonscattered light and $\tilde{S}_g$ be the glow-field component due to scattered light. Then

$$\tilde{S}(f_x,f_y) = \tilde{S}_g(f_x,f_y) + \tilde{S}_d(f_x,f_y) \ , \tag{24}$$

where

$$\tilde{S}_g(f_x,f_y) = (e^{-GZ_c} - e^{\alpha Z_c})\, e^{-BZ_c f} \ , \tag{25}$$

$$\tilde{S}_d(f_x,f_y) = e^{-\alpha Z_c} \ . \tag{26}$$

Taking the inverse transform of Eq. (24) gives

$$S(x,y) = S_g(x,y) + S_d(x,y) \quad , \tag{27}$$

where

$$S_g(x,y) = F^{-1}\left\{\tilde{S}_g(f_x,f_y)\right\} = (e^{-GZ_c} - e^{-\alpha Z_c})\, F^{-1}\left\{e^{-BZ_c f l}\right\} \quad , \tag{28}$$

$$S_d(x,y) = F^{-1}\left\{\tilde{S}_d(f_x,f_y)\right\} = e^{-\alpha Z_c}\, \delta(x,y) \quad . \tag{29}$$

$\delta(x,y)$ is the delta function with the following properties:

$$\delta(x,y) = \begin{cases} \infty, & x = y = 0 \\ 0, & \text{otherwise} \end{cases} \quad , \tag{30}$$

$$\iint_{-\epsilon}^{\epsilon} \delta(x,y)\, dx\, dy = 1 \text{ for any } \epsilon > 0 \quad .$$

Equation (17) expresses the image in the camera, H_2, in terms of a convolution of H_1 (the image that would be present in the absence of scattering and absorption effects in the reflected light from the object) with the point spread function S. This equation can now be rewritten in terms of two components, a glow-field component and a direct image component.

$$\begin{aligned} H_2(x,y) &= H_1(x,y) * S(x,y,z') \\ &= H_1(x,y) * \left[S_g(x,y,z') + S_d(x,y,z') \right] \\ &= H_1(x,y) * S_g(x,y,z') + H_1(x,y) * S_d(x,y,z') \\ &= H_g(x,y) + H_d(x,y) \quad . \end{aligned} \tag{31}$$

The glow-field component of the image, $H_g(x,y)$, is, using Eq. (28) for S_g,

$$H_g(x,y) = H_1(x,y) * \left[(e^{-GZ_c} - e^{-\alpha Z_c})\, F^{-1}\left\{e^{-BZ_c f l}\right\} \right] \quad . \tag{32}$$

Since $(e^{-GZ_c} - e^{-\alpha Z_c})$ is a constant, independent of x and y in the present form, it can be pulled out of the convolution giving

$$H_g(x,y) = (e^{-GZ_c} - e^{-\alpha Z_c}) \left[H_1(x,y) * F^{-1} \left\{ e^{-BZ_c f l} \right\} \right] . \tag{33}$$

According to Eq. (33) the glow-field calculation consists of attenuating each point in H_1 by $(e^{-GZ_c} - e^{-\alpha Z_c})$ and redistributing the remaining irradiance by convolution with the function shown. Thus the glow-field component is a blurred version of the object reflectance map. It does carry object detail in a degraded form. The amount of blur depends on the constant B and the distance Z_c.

In the same fashion the direct image component, $H_d(x,y)$, upon use of Eq. (29) for S_d, is

$$H_d(x,y) = H_1(x,y) * \left[e^{-\alpha Z_c} \delta(x,y) \right] = e^{-\alpha Z_c} H_1(x,y) . \tag{34}$$

This is an unblurred image, attenuated only by $e^{-\alpha Z_c}$.

As was previously stated, part of the shift variant property of the point spread function is due to increased path length for off-axis points, leading to greater attenuation and scattering. The expressions for H_g and H_d in Eqs. (33) and (34) contain attenuation factors proportional to the path length Z_c, which is the object plane to camera distance. These factors are multipliers of the undegraded iradiance array H_1. Therefore these factors can be modified to include the correct amount of attenuation for off-axis points by replacing Z_c by ρ, the distance from the camera to a point on the object plane. Equations (34) and (35) then become

$$H_g(x,y) = (e^{-G\rho} - e^{-\alpha\rho}) \left[H_1(x,y) * F^{-1} \left\{ e^{-BZ_c f l} \right\} \right] , \tag{35}$$

$$H_d(x,y) = e^{-\alpha\rho} H_1(x,y) , \tag{36}$$

where

$$\rho = (x'^2 + y'^2 + Z_c^2)^{1/2} , \tag{37}$$

H_1 is given by Eq. (13) on page 8, and the relationship between the image plane coordinates (x,y) and the space coordinate (x',y') in H_1 are given by Eq. (1). For clarification, the method of computation $H_g(x,y)$ would be as follows. The H_2 array is first weighted by $(e^{-G\rho} - e^{-\alpha\rho})$. The convolution is then accomplished by Fourier transforming the result, multiplying by $e^{-BZ_c f l}$ and then inverse transforming the product.

By applying the proper attenuation for off-axis points, one of the major approximations of the Fourier technique has been eliminated for the model of the optical transfer function proposed here. Only the increased spread of off-axis points in the glow-field due to greater path length and camera distortion of the glow-field pattern for off-axis points is neglected.

3.2 IRRADIANCE COMPONENTS DUE TO BACKSCATTERED LIGHT

COMPONENT DUE TO A SINGLE SLAB

The backscatter irradiance component in the camera image plane is due to light from the source scattered towards the camera by the water volume in front of the receiver. Consider an elemental volume $\Delta V'$ at (x',y',z') point in the water irradiated by the source irradiance $H_s(x',y',z')$. The geometry is shown in Figure 7. The radiant intensity of the light scattered toward the camera $J(x',y',z')$ is

$$J(x',y',z') = \sigma(\beta)\, H_s(x',y',z')\, \Delta V' \text{ (watts/steradian)} \tag{38}$$

where $\sigma(\beta)$ is the volume scattering function, and β is the angle between the incoming beam and the receiver, as shown in Figure 7. It should be noted that this equation is an approximation since there is actually an angular distribution of flux at (x',y',z') due to scattering between the source and the point, and to the finite size of the source. Thus at a given scattering volume there is a distribution of scattering angles β. Since the volume scattering function varies with β Eq. (38) contains some error. The magnitude of the error is unevaluated at this time.

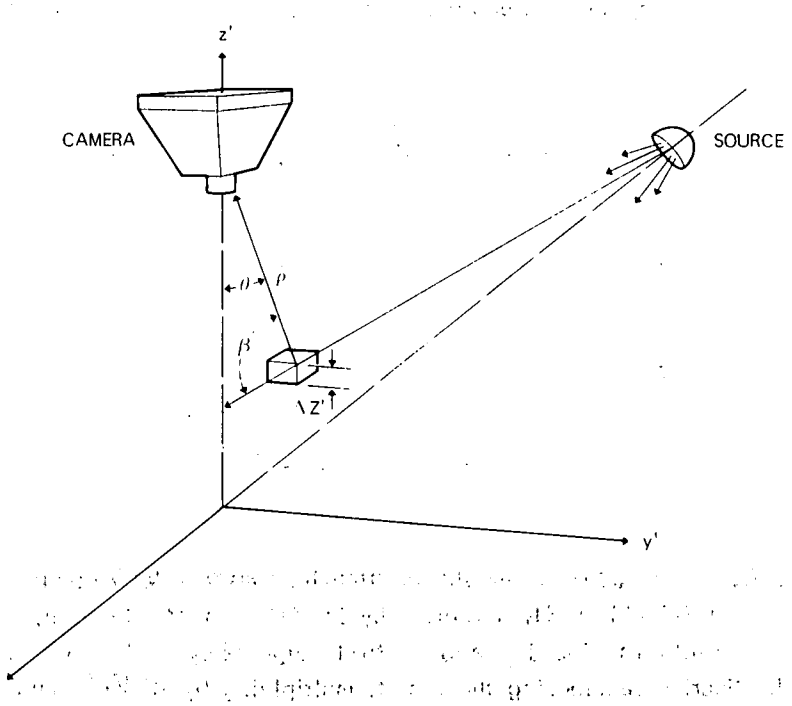

Fig. 7. An elemental backscatter volume.

As in the derivation for light reflected from the object, we initially consider the camera image of this irradiated volume of water as if there were no further scattering between that volume and the camera. The flux received and transmitted by the camera lens is

$$P_2(x',y',z') = J(x',y',z')\,\Delta\Omega\,(x',y',z')\,T_\ell \quad , \tag{39}$$

where T_ℓ is the transmittance of the lens, and $\Delta\Omega_L$ is the solid angle subtended by the lens,

$$\Delta\Omega\,(x',y',z') = \frac{\pi D^2 \cos\theta\,(x',y',z')}{4\rho^2\,(x',y',z')} \quad . \tag{40}$$

Combining Eqs. (38) and (40) into (39) gives

$$P_2(x',y',z') = \frac{\sigma(\beta)\,H_s(x',y',z')\,\pi D^2\cos\theta\,(x',y',z')\,T_\ell\,\Delta A'\,\Delta Z'}{4\rho^2\,(x',y',z')} \quad . \tag{41}$$

Here the substitution has been made $\Delta V' = \Delta A'\,\Delta Z'$ where $\Delta A'$ is the elemental area and $\Delta Z'$ is the elemental thickness of the scattering elemental volume. The flux given by Eq. (41) is imaged in the receiver image plane into an area $m_b^2 \Delta A'$, where m_b is the magnification for the backscatter plane. The receiver is focused on the object plane so that the image plane distance I is

$$I = \frac{F_\ell\ Z_c}{Z_c - F_\ell} \tag{42}$$

as before, so that m_b is

$$m_b = \frac{I}{(Z_c - z')} = \frac{F_\ell\ Z_c}{(Z_c - F_\ell)\,(Z_c - z')} \quad . \tag{43}$$

The image plane coordinates (x,y) are now related to space coordinates (x',y',z') through m_b given in Eq. (43). Since m_b is a function of z', we denote the image plane coordinates in the backscatter calculation by (x_b,y_b) where

$$x_b = m_b x' \quad , \tag{44}$$

$$y_b = m_b y' \quad . \tag{45}$$

The image plane irradiance $H_3(x_b,y_b)$ is now found by dividing Eq. (41) by $m_b^2 \Delta A'$. The result of doing this and substituting in the expression for m_b from Eq. (43) gives

$$H_3(x_b,y_b) = \frac{\sigma(\beta)\, H_s(x',y',z')\, \pi D^2 \Delta Z' \cos\theta(x',y',z')\,(Z_c - z')^2\, T_\ell}{4\rho^2(x',y',z')\, F^2_\ell} \cdot \left(\frac{Z_c - F_\ell}{Z_c}\right)^2 \quad . \tag{46}$$

Using $(Z_c - z')^2/\rho^2 = \cos^2\theta$ and $D/F_\ell = 1/f\#$ Eq. (46) becomes

$$H_3(x_b,y_b) = \frac{\sigma(\beta)\, H_s(x',y',z')\, \pi \Delta Z' \cos^3\theta(x',y',z')\, T_\ell}{4\, f\#^2} \cdot \left(\frac{Z_c - F_\ell}{Z_c}\right)^2 \quad . \tag{47}$$

The attenuation and scattering effects of the water on the light scattered from the elemental slab can now be obtained by convolving Eq. (47) with the water point spread function. This can be done by breaking the point spread function into a direct component and a glow-field component in exactly the same fashion as was done for the object reflected light. The same approximations are involved in doing the convolution by Fourier techniques as was previously discussed. Thus we can go directly to the final results by utilizing Eqs. (35) and (36) with $H_3(x_b,y_b)$ replacing $H_1(x,y)$, and $(Z_c - z')$ replacing Z_c as the distance from the camera to the plane being imaged. Thus the backscatter component due to a single slab, $H_b(x,y)$ is

$$H_b(x_b,y_b) = (e^{-G\rho} + e^{-\alpha\rho})\, H_3(x_b,y_b) * F^{-1}\left\{ e^{-B(Z_c - z')\, f\, l} \right\} + e^{-\alpha\rho}\, H_3(x_b,y_b) \quad , \tag{48}$$

where

$$\rho = \left[x'^2 + y'^2 + (Z_c - z')^2 \right]^{1/2} \quad . \tag{49}$$

EFFECT OF DEFOCUSED IMAGING

H_b is considered to be recorded in the image plane associated with the object so that the backscatter plane is actually imaged out of focus. To be more rigorous H_b should then be convolved with the defocus point spread function. As shown in Appendix I, using a geometrical optics approximation, the angular diameter of the defocus blur circle θ_d due to a point source located a distance of $Z_c - z'$ from a lens of diameter D which is focused on a plane at a distance of Z_c is

$$\theta_d = D \left[\frac{z'}{Z_c(Z_c - z')} \right] \text{ (Radians)} . \tag{50}$$

Whether or not the convolution is necessary for simulating the effect of defocus on H_b depends on the angular size of θ_d with respect to the angular size of the illuminated portion of the water slab at a distance of $(Z_c - z')$ from the camera. For example, let D = 25mm, Z_c = 10 meters, and z' = 9.5 meters. Then $\theta_d = 2.72°$. Now if the source were a 30° source and located in a plane with the camera, the volume of water illuminated at .5 meters from the camera would be somewhat larger than 30°, depending on beam spread and the horizontal separation of the source and camera. In this case the angular size of the beam pattern as seen by the camera is much larger than θ_d and the convolution could be ignored. In those cases where the source produces a very narrow beam then the convolution may be important.

For completeness we include the defocus convolution. In the image plane the defocus blur circle has the diameter d given by

$$d = l\theta_d = \frac{D F_\ell z'}{(Z_c - z')(Z_c - F_\ell)} , \tag{51}$$

Thus the defocus point spread function S_{bc} is given by

$$S_{bc}(x_b, y_b) = \left\{ \begin{array}{l} 1, \ (x_b^2 + y_b^2)^{1/2} < d/2 \\ \\ 0, \ (x_b^2 + y_b^2)^{1/2} > d/2 \end{array} \right\} . \tag{52}$$

The convolved function H_b' is given by

$$H_b'(x_b, y_b) = H_b(x_b, y_b) * S_{bc}(x_b, y_b) . \tag{53}$$

The convolution in Eq. (53) is best done by multiplication in the frequency domain by the Fourier transform of S_{bc} which is

$$F\left\{S_{bc}(x_b,y_b)\right\} = \frac{J_1\left(\frac{df}{2}\right)}{\left(\frac{df}{2}\right)} \quad , \tag{54}$$

where J_1 is a Bessel function of the first kind, order one and f is the spatial frequency variable. Thus

$$H_b'(x_b,y_b) = \left\{(e^{-G\rho} + e^{-\alpha\rho})\left[H_3(x_b,y_b) * F^{-1}\left\{e^{-B(Z_c - z')\,f\,l}\right\}\right]\right.$$

$$\left. + e^{-\alpha\rho}\, H_3(x_b,y_b)\right\} \quad * F^{-1}\left\{\frac{J_1\left(\frac{df}{2}\right)}{\left(\frac{df}{2}\right)}\right\} \quad . \tag{55}$$

THE TOTAL BACKSCATTER IRRADIANCE

The total backscatter irradiance component due to the entire water volume between the object and the receiver is found by adding the contributions from each slab. The number of slabs of thickness $\Delta Z'$ in the distance Z_c is $Z_c/\Delta Z'$ where $\Delta Z'$ is chosen to make this quantity an integer. $\Delta Z'$ must be chosen small enough that the distance along a line from the lens to the edge of the fold of view is a fraction of an attenuation length between adjacent slabs. The distance to the center of each of the slabs is $z' = \Delta Z'(n - 1/2)$ where n is the slab number. The total backscatter irradiance $H_{bt}(x,y)$ is then

$$H_{bt}(x,y) = \sum_{n=1}^{Z_c/\Delta Z'} H_b'\left\{x_b,y_b,\left[z' = \Delta Z'(n - 1/2)\right]\right\} \quad ,$$

$$x_b = m_b x' \, , \tag{56}$$

$$y_b = m_b y' \, ,$$

$$m = 1/(Z_c - z') \quad .$$

For convenience all terms of Eq. (56) are shown together in Appendix B, page B-3.

3.3 INCLUSION OF CAMERA PROPERTIES

At this point the three image components, direct, glow, and backscatter irradiance, do not include any spatial blurring of the image which would result from lens diffraction and aberration effects, sensor resolution, and temporal bandwidths of TV systems. In some cases these are significant factors, particularly sensor resolution. Each of these degrading factors can be described by a point spread function. The effect of the degrading factors can be simulated by convolving the total image, which is the sum of the three image components, with the point spread function associated with each factor. If the point spread functions are shift invariant then the convolution process is most easily done, as before, by multiplication in the Fourier domain of the transform of the total image by the transform of the point spread function.

3.4 EXTENSION TO THREE DIMENSIONAL OBJECTS

When imaging three dimensional objects, the image analysis problem becomes more complex. However, the model can be modified to provide a formulation for numerical calculations on three dimensional objects.

The three dimensional object has a reflectance map which varies as a function of all three space coordinates (x',y',z'). To account for this we replace the reflectance map $R(x',y',0)$ in Eq. (13) by an equivalent reflectance map $R_e(x',y',0)$. This is a reflectance map which is a projection of the three dimensional object on a two dimensional plane. It contains all important effects such as perspective, hiding of surfaces, shadowing, and specular reflections associated with the particular camera-source-object geometry.

To account for change in irradiance over the object due to changes in height the source irradiance on the object in Eq. (13) is computed as $H_s(x'_w,y'_w,z'_w)$ rather than $H_s(x',y',0)$. The (x'_w,y'_w,z'_w) coordinates are at the intersection of the object with the line of sight from the camera to the $(x',y'\ 0'$ point on the equivalent reflectance map, as shown in Figure 8. This requires a knowledge of $w(x',y',0)$ which is the distance between the $(x',y',0)$ coordinate and the corresponding intersection point at (x'_w,y'_w,z'_w). This is an object dependent quantity. Also ρ in Eqs. (35) and (36) are replaced by $\rho - w$. This accounts for the variation in distance between the camera and object due to object depth.

Modification of the backscatter calculation to account for the presence of the object above the $z' = 0$ plane can also be done by use of the w parameter. For each (x',y',z') element in the calculation of H_3 in Eq. (47) the corresponging $(x',y',0)$ location which lies on the projection of the line of sight from the camera to the (x',y',z') point is computed. The $w(x',y',0)$ associated with that point then allows a determination to be made as to whether the (x',y',z') point is inside or outside of the object. If it is outside then the calculation continues normally. If it is inside then H_3 is made equal to zero for that point.

Factors not accounted for by these modifications are change in the spread of the point spread function across the object due to change in object height, change in focus across the object due to change in object height and changes in irradiance of the water and object due to light reflected from the object.

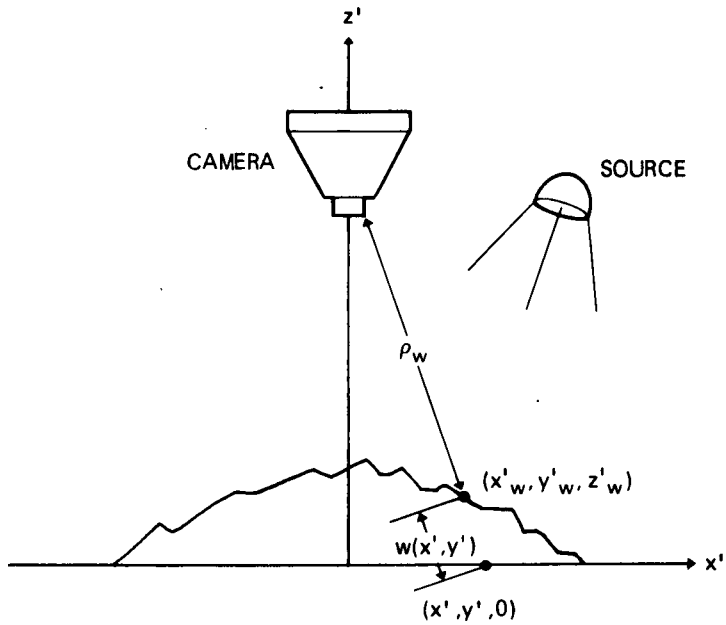

Fig. 8. Parameters used in extension to three dimensional objects.

4. APPLICATIONS

The basic numerical method for computer analysis of underwater camera systems has now been developed. Several different methods of using the method will be discussed and examples will be shown.

4.1 IMAGE PARAMETER CALCULATIONS

Exploration of the basic performance of a system as a function of water properties and geometry can be made by the calculation of simple image parameters based on the three image components: the direct, glow, and backscatter components. These calculations are done independently of a specific object reflectance map and an average reflectance is substituted for $R(x',y',0)$. Image degradation by the receiver lens and sensor are not included. This approach is useful for preliminary system analysis and design. Because reproduction of object detail is not required and because the source irradiance functions used usually contain little detail, these calculations can be done with small arrays. A program for low resolution calculations, SIMPRG, has been developed at the Visibility Laboratory. It computes all basic parameters over a 64 x 64 array size so that all calculations can be done on arrays residing in core memory. The program is structured so that parametric exploration of variables such as object distance, and source-camera spacing can be conveniently made. The parameters computed by SIMPRG are discussed below.

TOTAL IRRADIANCE

The total irradiance H_t at the surface of the sensor is, neglecting image degradation by the camera lens and sensor,

$$H_t(x,y) = H_d(x,y) + H_g(x,y) + H_{bt}(x,y) \quad . \qquad (57)$$

This quantity is useful for determining whether the flux level at the sensor is within the sensor's dynamic range.

CONTRAST TRANSMITTANCE

Contrast transmittance is a useful quantity for estimating the visual appearance of the image and for determining whether special processing will be needed to display the image to an observer with sufficient contrast for the human visual system. The variation of contrast transmittance over the field of view will also determine whether special processing of the image will be required to bring all regions of the image into a useful contrast range for the human visual system.

The concept of contrast is associated with the detection and recognition of spatially localized signals superimposed on a uniform background. Assume that the object has a detail which varies in irradiance in the image plane by ΔH_d from a uniform local background of H_{db}, so that H_d can be expressed as

$$H_d(x,y) = H_{db}(x,y) + \Delta H_d(x,y) \quad . \tag{58}$$

The inherent contrast is given by

$$C_o(x,y) = \frac{\Delta H_d(x,y)}{H_{db}(x,y)} \quad . \tag{59}$$

Thus

$$\Delta H_d(x,y) = C_o(x,y)\, H_{db}(x,y) \quad . \tag{60}$$

The assumption is made that the glow-field contains little image detail and that both the glow-field and backscatter components are uniform over the detail of interest. With addition of the glow-field and backscattering components the contrast is

$$C(x,y) = \frac{\Delta H_d(x,y)}{H_{db}(x,y) + H_g(x,y) + H_{bt}(x,y)} \quad . \tag{61}$$

The contrast transmittance C_t is the ratio of the actual contrast to the inherent contrast

$$C_t(x,y) = \frac{C(x,y)}{C_o(x,y)} = \frac{H_{db}(x,y)}{H_{db}(x,y) + H_g(x,y) + H_{bt}(x,y)} \quad . \tag{62}$$

In making calculations of C_t, H_{db} can be equated to the H_d associated with an average background reflectance or a smoothed reflectance map in which local variations (signals) have been reduced.

SIGNAL-TO-NOISE RATIO

The signal-to-noise ratio is a fundamental quantity in the analysis of the performance of systems. The signal-to-noise ratio indicates whether any useful information can be extracted from the image, even after contrast enhancement. The signal-to-noise ratio depends on the input to the sensor, the properties of the sensor and associated components, and the definition used for the signal-to-noise ratio. Here we use the signal-to-noise ratio for a single resolution element of area ΔA at the sensor surface. We assume that the sensor is an ideal quantum limited sensor, with quantum efficiency of μ. The signal is defined as the mean number of photo electrons that would be ejected from a photocathode surface in a time T due to an incremental signal irradiance of $C_o H_{db}$ where C_o is the inherent contrast of some detail on a locally uniform background of H_{db}. The number of signal electrons N_s is given by

$$N_s = \frac{C_o(x,y) H_{db}(x,y) \quad \Delta A \, T \, \mu \, \lambda}{hc} \quad , \tag{63}$$

where h is Planck's constant, λ is the wavelength of light, and c is the velocity of light. The average number of electrons emitted due to the irradiance from all components is found from a similar expression with the total irradiance H_t replacing $C_o H_{db}$. Assuming that the photoelectrons follow Poisson statistics the standard deviation of the fluctuation about the mean value is equal to the square root of the mean. Thus the noise component N_n due to the total irradiance at a resolution element is

$$N_n(x,y) = \left\{ \frac{\left[H_{db}(x,y) + H_g(x,y) + H_{bt}(x,y) \right] \quad \Delta A \, T \, \mu \, \lambda}{hc} \right\}^{1/2} \quad . \tag{64}$$

The signal-to-noise ratio SNR is then given by the ratio N_s / N_n:

$$SNR(x,y) = \frac{C_o(x,y) H_{db}(x,y)}{\sqrt{H_{db}(x,y) + H_g(x,y) + H_{bt}(x,y)}} \left(\frac{\Delta A \, T \, \mu \, \lambda}{hc} \right)^{1/2} \quad . \tag{65}$$

Note that in Eq. (65) $\mu\lambda/hc$ can be replaced by $S(\lambda)/e$ where $S(\lambda)$ is the spectral sensitivity of the sensor and e is the electron charge.

The signal-to-noise values as computed by Eq. (65) must be used with some caution. A good signal-to-noise ratio, as defined in Eq. (65), would be dependent upon the particular task the observer was expected to accomplish with the image. If the task was to detect a single picture element on a uniform background, then Eq. (65) would be a very useful quantity. If the observer was required to detect a uniform array of M resolution elements on a uniform background then Eq. (65) would be applicable by replacing ΔA with $M \cdot \Delta A$. If the image was due to a complex scene and the observer task was to identify objects in the scene, then Eq. (65) would be of little use. In this case a signal-to-noise ratio based on decision theory[7] would be more appropriate.

In addition temporal and spatial averaging processes of the human visual system could lead to effectively higher values of ΔA and T in the equation with corresponding higher values of signal-to-noise. Conversely, less than ideal characteristics of sensors (such as amplifier noise in TV systems, nonlinearities, etc.) could lead to lower signal-to-noise ratios.

EXAMPLE

To illustrate the use of the basic image parameter calculations, the results of a parametric study are presented in Figures 9 to 13. The system for which the calculations were performed consisted of a fairly broad beam source, emitting at a wavelength of 530 nanometers, an object of uniform reflectance of .1 and a camera. The camera was pointed straight down and the source was always pointed at the intersection of the camera axis with the $z' = 0$ plane. The horizontal separation between the source and the camera was varied from 0 to 8 meters in steps of 2 meters. The camera to object distance was varied from zero to 20 meters in steps of 4 meters. The source was always in the same plane as the camera. The source distribution is shown in Table C-I in Appendix C. Unit power output, i.e., 1 watt, was assumed. The water properties used were

$$\alpha = .25/\text{meter}$$

$$s/\alpha = .375$$

$$s = .09375$$

$$a = .15625$$

$$G = .195$$

The volume scattering function used is tabulated in Table C-II in Appendix C. The camera lens was assumed to have an f number of 2.8, a focal length of 27.5 millimeters and a transmittance of .75.

The output from the program used to make the calculations, SIMPRG, gives H_o, H_g, H_{bt}, H_t, C_t, and SNR as a function of position in the field for each configuration of the system. In addition it prints out the backscatter along the camera axis from each elemental backscatter slab. Thus a large amount of data is obtained for each system configuration. Only a representative part of the data will be shown here.

Figure 9 shows the magnitude of the three image components as a function of camera altitude and source-camera separation. It demonstrates the rather complicated relationships between the image plane components. For $Z_c = 4$ meters (1 attenuation length) the direct object component is much greater than the glow-field component. At $Z_c = 12$ meters (3 attenuation lengths) the two are nearly equal, and at $Z_c = 20$ meters (5 attenuation lengths) the glow-field is significantly larger than the direct component. For zero source-camera separation the backscatter component is the largest for all values of Z_c, but drops rapidly as the separation increases. For $Z_c = 4$ meters (1 attenuation length) the backscatter and direct image components are approximately equal. For $Z_c = 12$ meters (3 attenuation lengths) the backscatter is considerably larger and at $Z_c = 20$ meters it is much larger than the direct component. In going from $Z_c = 12$ to $Z_c = 20$ the backscatter component remains essentially constant.

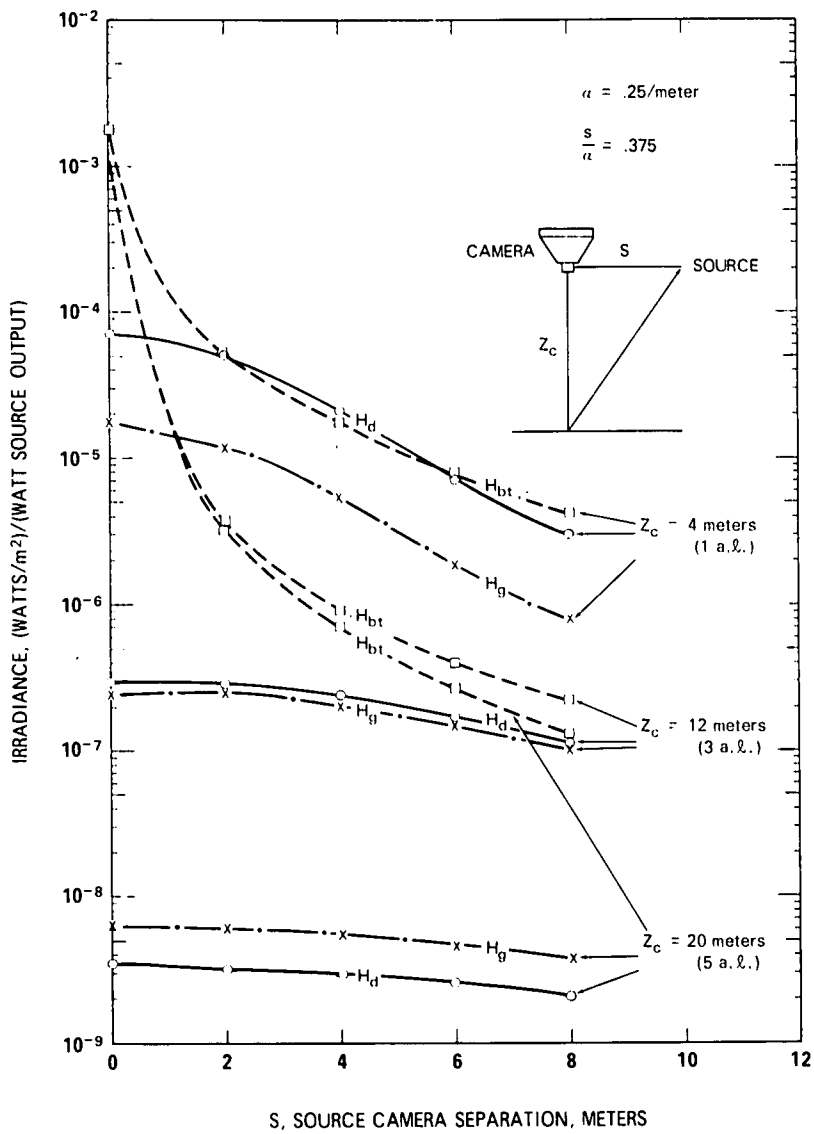

Fig. 9. On-Axis image plane irradiance components as a function of camera altitude and source-camera separation.

Figure 10 shows how the contrast transmittance varies as a function of camera altitude and source-camera separation. In general the contrast transmittance continues to increase as the source-camera separation is increased. The one exception occurs for Z_c = 4 meters, for which the contrast transmittance peaks at a separation of about 3 meters. The reason for the decrease beyond that point is, as can be seen in Figure 9, the direct image component decreases more rapidly than the backscatter component. This is probably due to decrease of object irradiance and the $\cos\gamma$ component in Eq. (4).

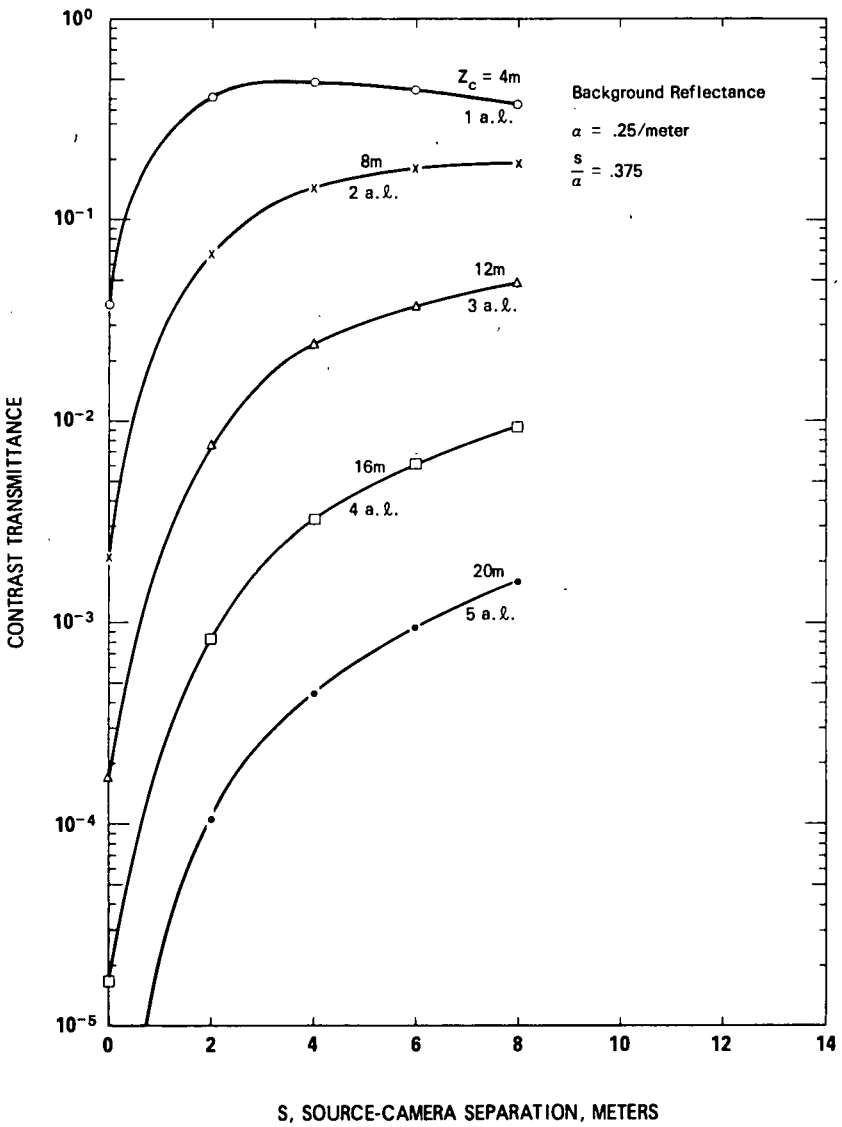

Fig. 10. On-Axis contrast transmittance as a function of camera-altitude and source-camera separation.

Figure 11 shows how the signal-to-noise ratio varies as a function of camera-altitude and source-camera separation. This data is for one watt output from the source and detail contrast of 1.0. For other source outputs the plotted values can be multiplied by the square root of the output to obtain signal-to-noise ratios for those outputs. For other contrasts the plotted values can be multiplied by the contrast. The signal-to-noise ratio is for a picture element size of 7.14×10^{-3} meters, which is 1/490 of a 35mm format. The 1/490 ratio comes from the fact that these are 490 active TV lines in a standard television frame. An integration time of .033 seconds, and a quantum efficiency of .15 at 530 nanometers was used.

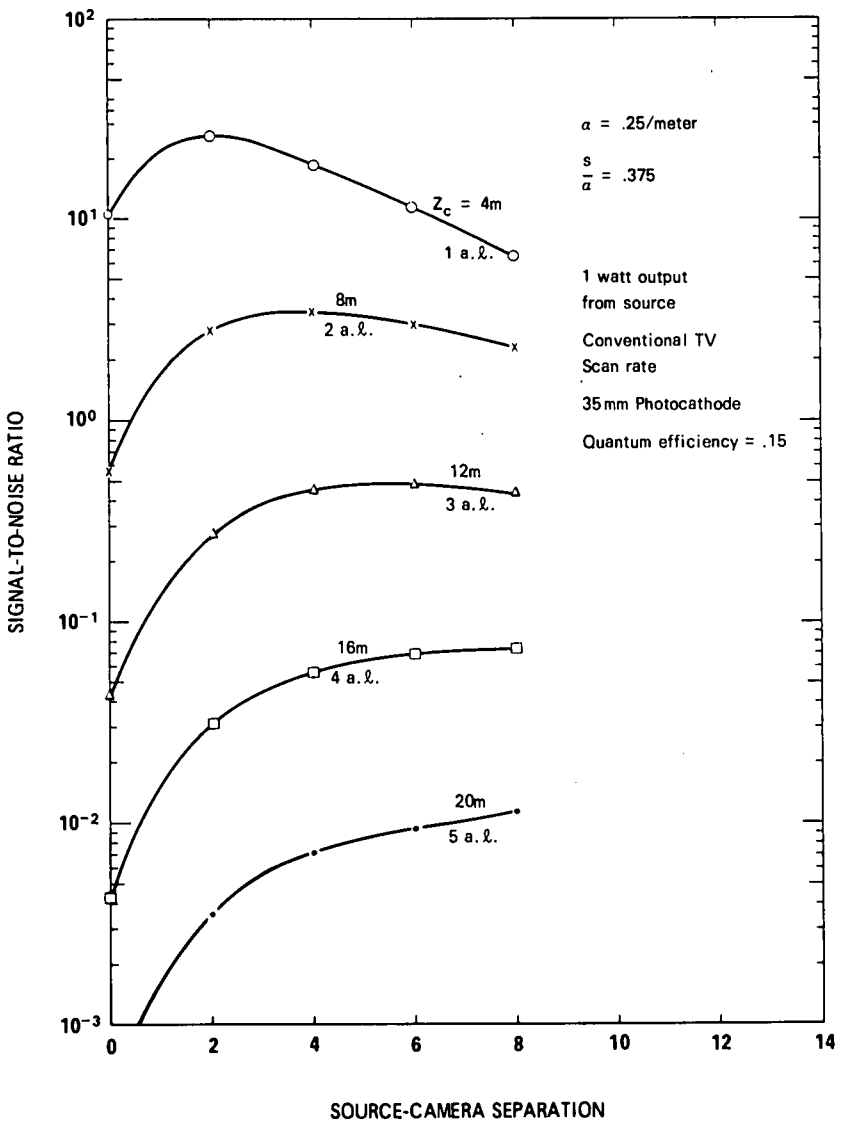

Fig. 11. On-Axis SNR for a single resolution element as a function of camera altitude and source-camera separation.

The signal-to-noise curves are similar to the contrast transmittance curves except they flatten out more rapidly with increasing separation and for Z_c = 4, 8, and 12 meters actually peak and then decrease with increasing separation. This is due to decreased irradiance at the object with increasing separation.

In the figures discussed so far, all data values have been for the center of the field of view of the camera. A set of curves could be drawn for each picture element in the field of view since the three image components vary in different ways across the field. To demonstrate this the contrast transmittance and signal-to-noise ratios for a horizontal line through the center of the field are plotted in Figures 12 and 13 for a camera distance of 12 meters and source-camera separations of 6, 4, 2, and 0 meters. Here it can be seen that these image parameters vary significantly over the field of view.

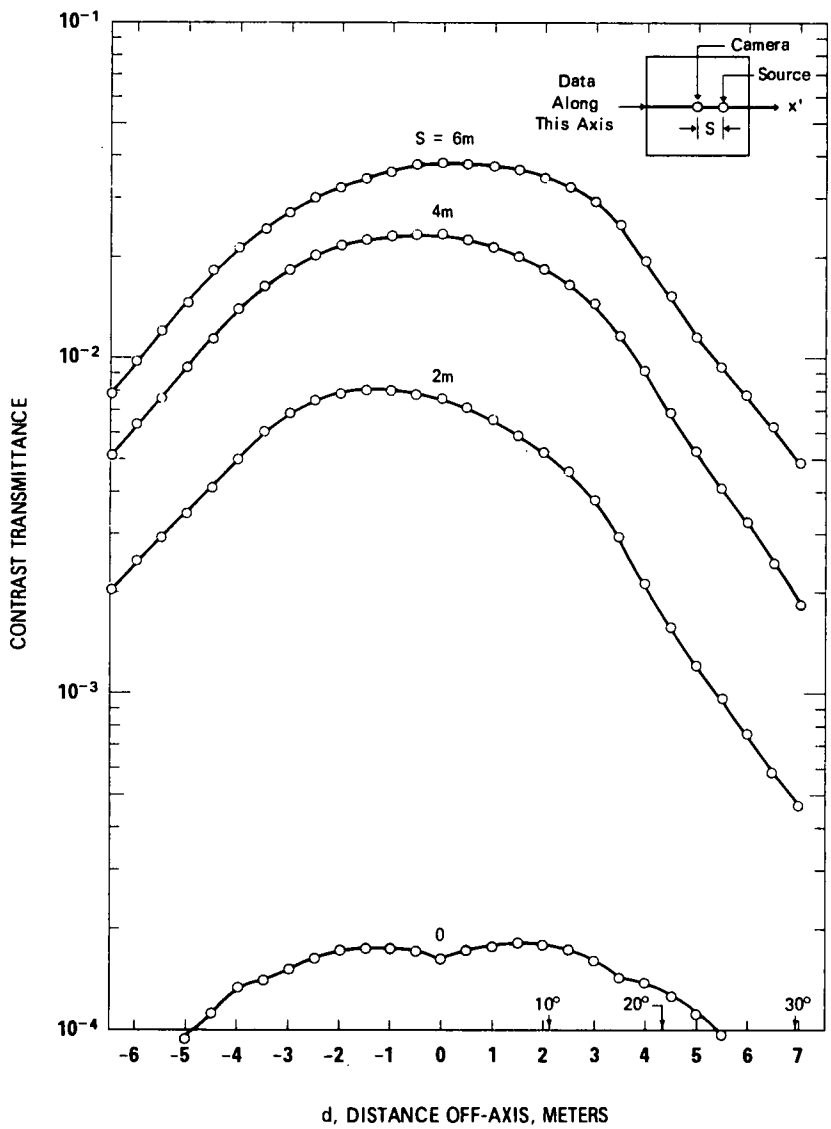

Fig. 12. Contrast transmittance as a function of location in field for Z_c = 12 meters, S = 6, 4, 2, 0 meters.

4.2 IMAGE SIMULATION

Calculation of basic image parameters as described in the previous section is a very useful approach for optimizing design. However, the question as to whether a system will be adequate to accomplish a specific task is often a complex question. Often specific classes of objects are involved, and the task of the observer may be to detect, or to classify, or to identify these objects so that the performance of the human visual system is an important part of the systems. Thus in some cases final evaluation of the system is best done by actual simulation of images. This can be done by computer simulation using the method that has been developed here.

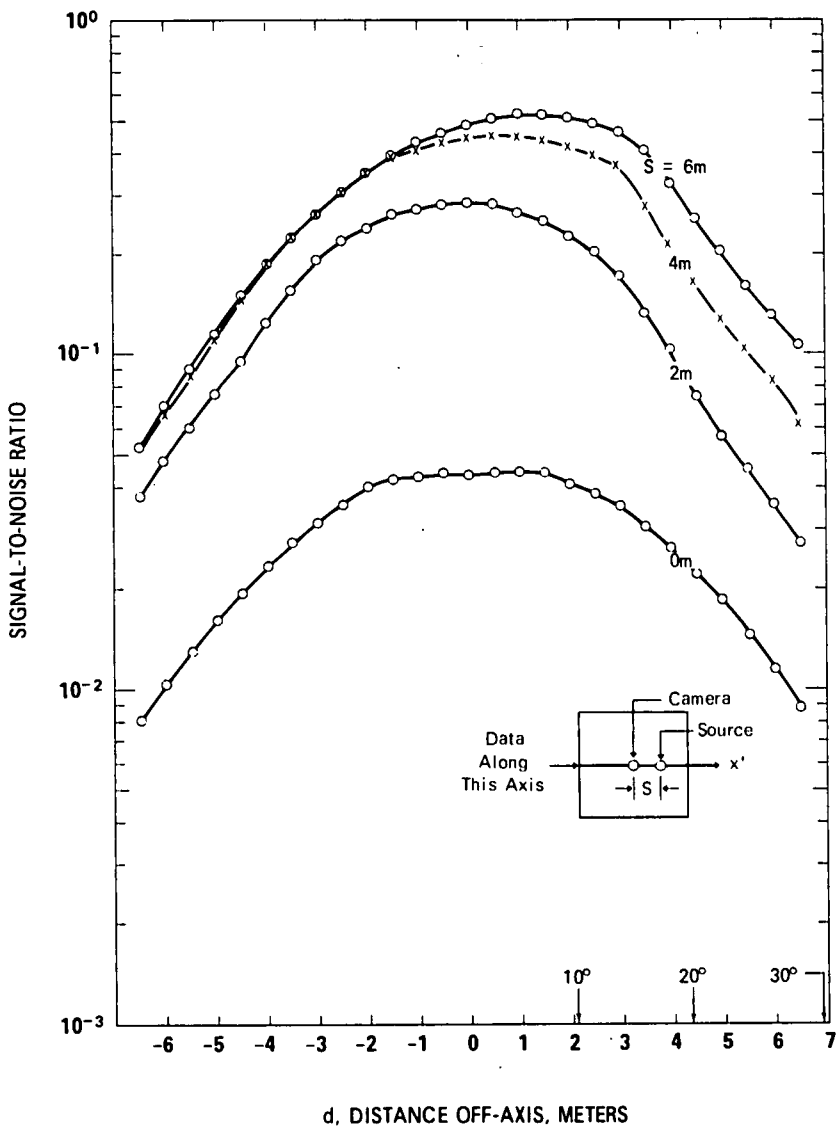

Fig. 13. Signal-To-Noise as a function of location in field for Z_c = 12 meters, S = 6, 4, 2, 0 meters.

One approach to the simulation procedure would be as follows. The direct and glow-field components are computed using a high resolution reflectance map in the calculations. This requires evaluation of Eqs. (35) and (36) using arrays large enough to match the sensor resolution. This calculation involves one forward and one inverse transform plus the application of off-axis weighting terms. The backscatter calculation which consists of many Fourier transform pairs, can usually still be done using small arrays with lower spatial resolution. The final total backscatter component can then be expanded by interpolation into the larger high resolution array size and then added to the direct and glow-field image components. Camera and sensor optical transfer functions effects are then put in by Fourier transform techniques, requiring another pair of Fourier transforms. Sensor noise is then superimposed. Finally, temporal bandwidth effects (for TV-type systems) can be put in by Fourier transform techniques, again requiring another transform pair.

At the Visibility Laboratory these operations are performed by use of the Laboratory's general purpose image processing system implemented on an IBM System 360/44. The largest convenient working array size for this system is 512 x 512.

A typical example of simulation of an underwater image is shown in Figures 14 and 15. Figure 14 shows the simulation of the three basic image plane components. Figure 15 shows simulation of shot noise for various source input powers and the result of application of standard and special processing techniques for contrast enhancement.

4.3 A SPECIAL PROBLEM

The method which has been developed can also be used to address special problems. As an example, we pose the following problem. Can images obtained at low altitude with one camera system be used to infer water properties with sufficient accuracy so that the performance of a completely different camera system operating at a higher altitude can be adequately predicted?

To address this question the basic image parameters were computed for two systems using program SIMPRG. The low altitude system, designated as system A, obtains pictures from an altitude of 8 meters. The source-camera separation is 1 meter. The high altitude system, system B, obtains pictures from an altitude of 32 meters and has a source-camera separation of 4 meters. The two systems use the same source. The radiant intensity disbribution of the source is tabulated in Appendix C.

The basic image parameters were calculated for both systems for waters with attenuation lengths of $1/\alpha$ = 6, 7, 8, 9, and 10 meters. Values of s/α = .212, G/α = .917, and B = .1 were used in all cases.

The approach in utilization of this data was to infer $1/\alpha$ by measuring contrast transmittance as a function of $1/\alpha$. Contrast transmittance versus $1/\alpha$ is shown in Figure 16 for both systems.

We now assume that images are taken with system A in water with $1/\alpha$ = 8 meters. Contrast measurements are made on these images. Then by use of the known curve of contrast transmittances versus $1/\alpha$, $1/\alpha$ can be determined. Due to errors in measurement and lack of knowledge of the object, errors in

(a) REFLECTANCE MAP

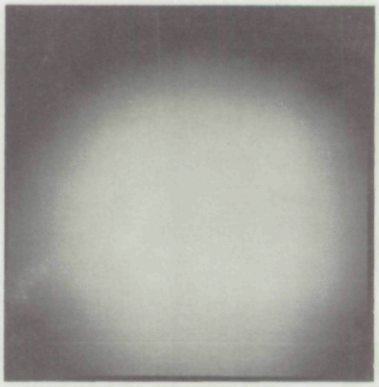

(b) OBJECT IRRADIANCE

(c) DIRECT IMAGE

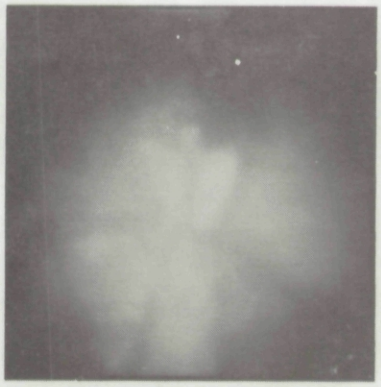

(d) GLOW-FIELD IMAGE

(e) BACKSCATTER IMAGE

(f) TOTAL IMAGE

Figure 14. Example of system simulation capability. Viewing distance is three attenuation lengths. The camera and source are assumed to be 12 meters above the object. The camera is centered on the object and the source is 4 meters in the minus-y direction from the camera. The object is a small boat anchor but a scale has been assumed to simulate an anchor with a shank length of 6.78 meters, corresponding to the anchor of a very large ship. The area represented by the picture is a 16 x 16 meter square. The computer array size is 512 x 512 picture elements. The water properties are: $1/\alpha = 4$ meters, $s/\alpha = .375$, $1/s = 10.7$ meters, and $1/G = 5.13$ meters. Note that the final image is dominated by backscatter and the anchor can barely be seen. See Figure 15 for enhanced images.

(a) The reflectance map, $R(x,y)$

(b) The irradiance on the object, $H_1(x,y)$

(c) The direct image irradiance, $H_d(x,y)$

(d) The glow-field image irradiance, $H_g(x,y)$. Note the object related structure in the glow-field image.

(e) The total backscatter image irradiance, H_{bt}

(f) The total image irradiance,

$$H_t(x,y) = H_d(x,y) + H_g(x,y) + H_{bt}(x,y)$$

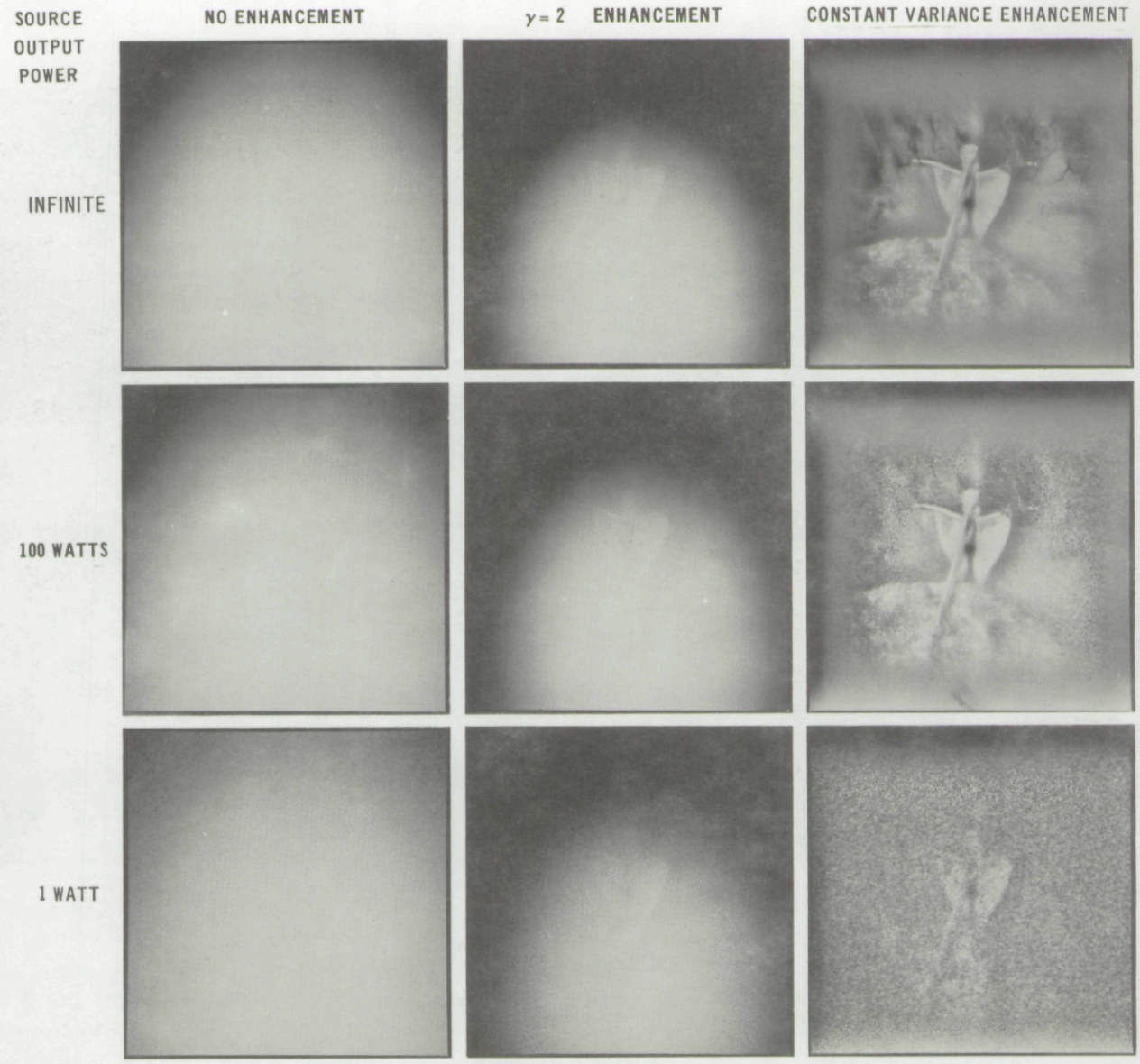

Figure 15. Example of simulation of sensor properties and special enhancement processing. The beginning image (upper left) is a repetition of the total image in Fig. 14(f). Assumed optical system parameters: f# = 3.5, focal length = 27 mm, transmittance = .75. Assumed sensor properties: photoelectric sensor with quantum efficiency of 0.15 at 500 nanometers, integration time of .033 seconds, and useful sensor area of 35 x 35 millimeters. The assumption has been made that the sensor modulation transfer function and video modulation transfer function are approximately unity over the spectrum of the image.

1st row: infinite source power output. **2nd row:** 100 watt source power output. **3rd row:** 1 watt source power output.

1st column: H_t added with Poisson shot noise associated with a quantum limited sensor. The ratio of the image signal to the rms noise is directly proportional to the square root of the image signal power. Thus for infinite source power no noise is apparent.

2nd column: Same as first column but with data squared to enhance contrast. Anchor is visible but nonuniform illumination causes part of scene to drop out.

3rd column: First column image after application of a constant variance filtering process. This is a space-variant process which subtracts the local mean and divides by the local standard deviation. This then allows a large amount of contrast enhancement to be applied. These images demonstrate that sensor shot noise is the ultimate limitation in extracting information from low contrast images. Compare the upper right picture in this figure with Fig. 14(c).

measurement of contrast transmittance reflect into errors of $1/\alpha$. The contrast transmittance is the contrast in the recorded image divided by the inherent contrast. Therefore the problem reduces to measuring the contrast in the recorded image and determining the inherent contrast. Errors in measurement of the contrast of the recorded image are caused by noise in the image and uncorrected nonlinearity of the sensor. Errors in the inherent contrast will be caused mainly by a lack of knowledge of the characteristics of the object. Without pursuing these errors in detail, let us assume that the contrast transmittance of the water can be measured with an r.m.s. error of 10%. On Figure 16 a ± 10% error in contrast transmittance around the contrast transmittance for $1/\alpha$ = 8 meters is shown. When this error band is reflected from the contrast transmittance graph for system A, it intercepts the absicca at $1/\alpha \approx 7.1$ and $1/\alpha$ 8.9. Reflecting the error band off of the contrast transmittance graph for system B results in a contrast transmittance uncertainty for system B, which ranges from 3×10^{-3} to 1.6×10^{-2}. Thus an r.m.s. error of 10% in measuring

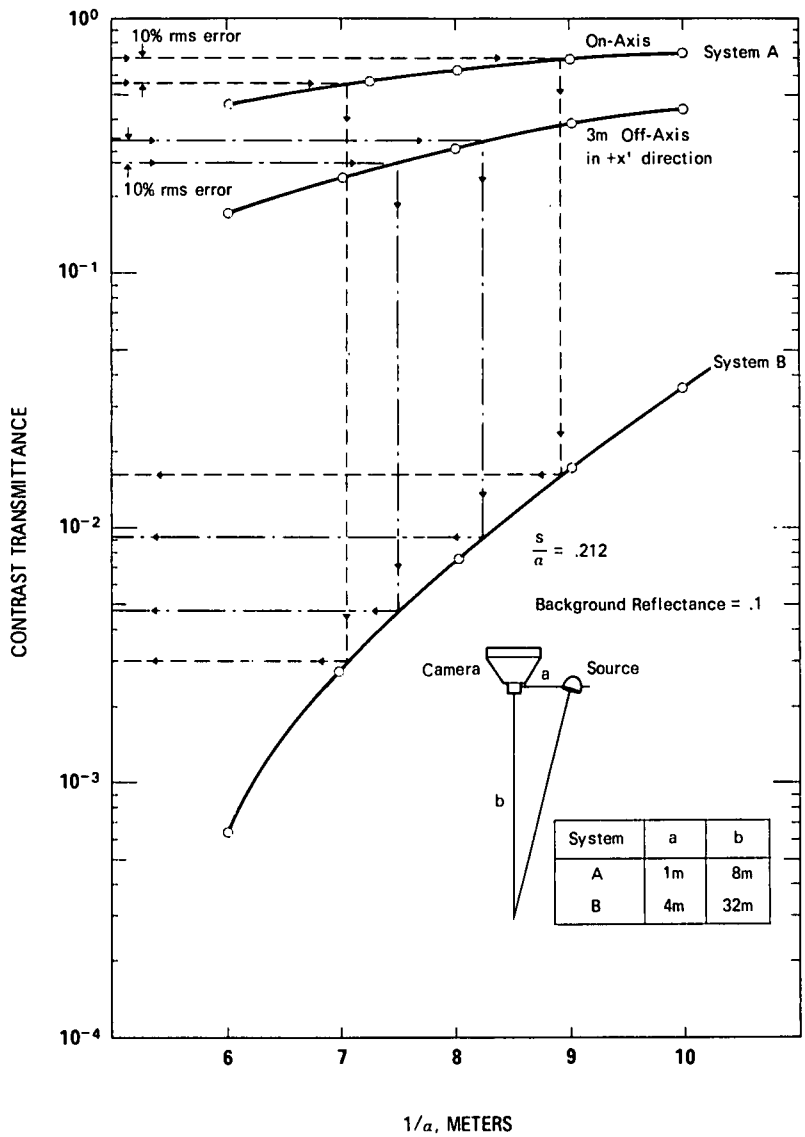

Fig. 16. Contrast transmittance versus range for two systems.

contrast transmittance with system A has resulted in a contrast transmittance performance estimate which ranges over a factor of 5.3 or more. This would not seem to be a satisfactory estimate of the performance of system B.

A smaller error is obtained if the contrast transmittance at the right edge of the field is used. This is more sensitive to $(1/\alpha)$ since the line of sight passes through a more intense part of the beam. Here an r.m.s. error of contrast transmittance of 10% in system A converts into a predicted contrast transmittance range which covers a factor of 1.9. This is nearly one third of the error with the on-axis contrast transmittance.

The problem of determining water properties from images is actually much more complicated than the present example would indicate. A great deal was assumed about the water. It was assumed that the volume scattering function was known within a multiplicative constant, and that s, a, and G were tied to α through multiplicative constants. Thus the only unknown was α. In the actual case the shape of the volume scattering function, α, s/α, and G/α may all be unknown quantities. This would greatly complicate the analysis and undoubtedly make errors in measurement propagate into even larger errors of inferred water properties.

It should also be noted that the ability to infer water properties with system A in order to accurately predict the performance of system B in the same water greatly depends on the difference between the two systems. In the example shown here the small errors in measurement of contrast transmittance with system A propagated into large errors of predicted contrast transmittances for system B. This was due to the large difference in slopes of the contrast transmittances versus $1/\alpha$ curves. The difference in slopes was due primarily to the difference in altitudes of the two systems. Thus if system A was lower in altitude or system B was higher in altitude the ability to predict performance of B on the basis of the performance of A would be further degraded.

5. REFERENCES

1. S. Q. Duntley, J. Opt. Soc. Amer., **53** 214 (1963).

2. The beam spread function is equivalent to the off-axis irradiance of a collimated beam discussed in reference 1.

3. Joseph W. Goodman, "Introduction to Fourier Optics, p 18, McGraw Hill, San Francisco, 1968.

4. S. Q. Duntley, "Underwater Lighting by Submerged Lasers and Incandescent Sources," Scripps Institution of Oceanography, SIO Ref. 71-1 (1971). Available from DDC, No. AD 730721.

5. Reference 3, p 18 and 114.

6. Reference 3, p 10.

7. J. L. Harris, J. Opt. Soc. Amer., **54** 606 (1964).

APPENDIX A

CALCULATION OF BLUR CIRCLE DIAMETER

Let a lens of focal length F be focused on an object at a distance of Z_c. The diameter of the defocus blur circle due to a point at a distance of z will be calculated.

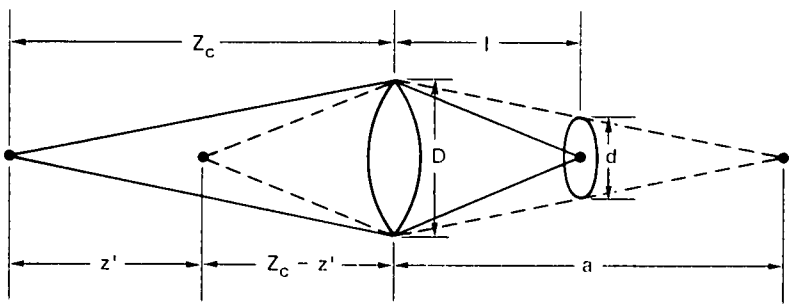

The image plane distances "l" and "a" for objects at Z_c and z' are

$$l = \frac{Z_c F_\ell}{Z_c - F_\ell}$$

$$a = \frac{(Z_c - z') F_\ell}{(Z_c - z' - F_\ell)}$$

By similar triangles the diameter d of the blur circle at a distance of I from a lens of diameter D due to a point at z' is

$$d = D\left(\frac{a - I}{a}\right) .$$

The angular diameter θ_d is found by dividing by I.

$$\theta_d = \frac{d}{I} = D\left(\frac{a - I}{aI}\right) = D\left(\frac{1}{I} - \frac{1}{a}\right) .$$

After substituting in the values of I and a this reduces to

$$\theta_d = D\,\frac{z'}{Z_c(Z_c - z')} .$$

APPENDIX B

SUMMARY OF EQUATIONS

For convenience the equations developed in this report are summarized here.

DIRECT IMAGE PLANE COMPONENT

$$H_d(x,y) = \frac{H_s(x',y',0)\, R(x',y',0) \cos^4\theta(x',y',0) \cos\gamma(x',y',0)\, T_\ell}{4f\#^2} \cdot \left(\frac{Z_c - F_\ell}{Z_c}\right)^2 \cdot e^{-\alpha\rho}$$

where

H_s = source irradiance at image plane

R = object reflectance

θ = $\arctan (x^2 + y^2)^{1/2} / Z_c$

γ = angle between perpendicular to object plane at point (x,y,Z_c) and source

ρ = $(x'^2 + y'^2 + Z_c^2)^{1/2}$

Z_c = distance from receiver to object

F_ℓ = focal length of lens

α = volume attenuation coefficient

I = image plane distance = $Z_c F_\ell / (Z_c - F_\ell)$

f# = f number of optical system

x = mx'

y = my'

m = optical magnification = $1/Z_c$

GLOW-FIELD IMAGE PLANE COMPONENT

$$H_g(x,y) = (e^{-G\rho} - e^{-\alpha\rho}) \cdot \left(\frac{Z_c - F_\ell}{Z_c}\right)^2 \left[\frac{H_s(x',y',0)\, R(x',y',0)\, \cos^4\theta(x',y',0)\, \cos\gamma(x',y',0)\, T_\ell}{4f\#^2}\right]$$

$$* \; F^{-1}\left\{e^{-BZ_c f\, l}\right\}$$

where

H_s = source irradiance at image plane

R = object reflectance

θ = arc tan $(x^2 + y^2)^{1/2}/Z_c$

γ = angle between perpendicular to object plane at point (x',y') and source

Z_c = distance from receiver to object

T_ℓ = transmittance of lens

F_ℓ = focal length of lens

ρ = $(x'^2 + y'^2 + Z_c^2)^{1/2}$

G = an attenuation coefficient associated with a point source

α = volume attenuation coefficient

B = empirical constant related to scattering

f = spatial frequency = $(f_x^2 + f_y^2)^{1/2}$

f_x, f_y = horizontal and vertical spatial frequencies

l = image plane distance from lens = $Z_c F_\ell / (Z_c - F_\ell)$

f# = f number of optical system

x = mx'

y = my'

m_b = optical magnification = $1/Z_c$

$*$ = denotes convolution

BACKSCATTER IMAGE PLANE COMPONENT

$$H_{bt}(x,y) = \sum_{n=1}^{Z_c/\Delta Z' n} H_b' \left[x_b, y_b, z' = \Delta Z' \left(n - \frac{1}{2}\right) \right] ,$$

where

$$H_b'(x_b,y_b,z') = H_b(x_b,y_b,z') * F^{-1} \left\{ \frac{J_1(df/2)}{(df/2)} \right\}$$

$$d = l\theta_d = \frac{D F_\ell z'}{(Z_c - z')(Z_c - F_\ell)}$$

$$H_b(x_b,y_b,z') = (e^{-G\rho} + e^{-\alpha\rho}) \left\{ H_3(x_b,y_b,z') * F^{-1} \left[e^{-B(Z_c - z')/f} \right] \right\} + e^{-\alpha\rho} H_3(x_b,y_b,z')$$

$$H_3(x_b,y_b,z') = \frac{\sigma(\beta) H_s(x',y',z') \pi \Delta Z' \cos^3\theta T}{4f\#^2} \left(\frac{Z_c - F}{Z_c} \right)^2$$

$$z' = \Delta Z' \left(n - \frac{1}{2}\right)$$

$$x_b = m_b x'$$

$$y_b = m_b y'$$

$$m_b = 1/(Z_c - z')$$

and

$\sigma(\beta)$ = volume scattering function

β = angle between receiver and source at point (x,y,z)

H_s = source irradiance at (x',y',z')

$\Delta Z'$ = thickness of elemental slab

θ = arc tan $(x'^2 + y'^2)^{1/2}/z'$

T_ℓ = transmittance of lens

Z_c = distance to plane on which receiver lens is focused

F_ℓ = focal length of lens

f# = f number of lens

G = an attenuation coefficient associated with a point source

α = volume attenuation coefficient (Alpha)

$\rho = \left[(x'^2 + y'^2 + (Z_c - z')^2\right]^{1/2}$

B = empirical glow-field spread constant

f = spatial frequency = $(f_x^2 + f_y^2)^{1/2}$

(f_x, f_y) = horizontal and vertical spatial frequency coordinates

I = image plane distance for object at $Z_c = Z_c F_\ell / (Z_c - F_\ell)$

d = diameter of defocus blur circle

D = diameter of lens

F_ℓ = focal length of lens

J_1 = first order Bessel function of the first kind

$*$ = denotes convolution

F^{-1} = denotes inverse Fourier transform

TOTAL IMAGE PLANE IRRADIANCE

$$H_t(x,y) = H_d(x,y) + H_g(x,y) + H_{bt}(x,y)$$

CONTRAST TRANSMITTANCE

$$C_t(x,y) = \frac{H_{db}(x,y)}{H_{db}(x,y) + H_g(x,y) + H_{bt}(x,y)}$$

where

H_{db} = local average of direct image irradiance component.

SIGNAL-TO-NOISE RATIO

$$SNR(x,y) = \frac{C_o(x,y)\, H_{db}(x,y)}{\sqrt{H_{db}(x,y) + H_g(x,y) + H_{bt}(x,y)}} \left(\frac{\Delta A\, T\, \mu\, \lambda}{hc} \right)^{1/2}$$

$$= \frac{C_o(x,y)\, H_{db}(x,y)}{\sqrt{H_{db}(x,y) + H_g(x,y) + H_{bt}(x,y)}} \left(\frac{\Delta A\, T\, S(\lambda)}{e} \right)^{1/2}$$

where

C_o = inherent contrast at object

H_{db} = local average of object irradiance component

ΔA = area of resolution element at sensor

T = integration time of sensor

μ = quantum efficiency of sensor

λ = wavelength of light

h = Planck's constant

c = velocity of light

$S(\lambda)$ = spectral sensitivity of photocathode surface

e = electron charge.

APPENDIX C

DATA

Table C-I

Relative Beam Radiant Intensity of Source Used in Parametric Calculations

	Horizontal		Vertical	
θ (Degrees)	Left	Right	Up	Down
0	1.000	1.000	1.000	1.000
5	0.972	0.975	0.995	0.981
10	0.947	0.951	0.965	0.932
15	0.867	0.874	0.908	0.790
20	0.520	0.502	0.766	0.601
25	0.422	0.419	0.571	0.418
30	0.358	0.347	0.364	0.340
35	0.293	0.288	0.289	0.302
40	0.236	0.233	0.252	0.258
45	0.189	0.187	0.221	0.212
50	0.155	0.154	0.180	0.173
55	0.124	0.123	0.144	0.142
60	0.099	0.098	0.112	0.110
65	0.077	0.076	0.084	0.083
70	0.057	0.056	0.060	0.062

Table C-II

Volume Scattering Function, $\sigma(\beta)$ Used in Numerical Calculations*

$$\sigma(\beta) = f(\beta)/f(90°) \cdot s/225$$

where s is the total scattering coefficient.

β	$f(\beta)/f(90°)$
0	4910
5	1560
10	411
15	177
20	84.4
25	45.6
30	27.6
35	17.3
40	11.5
45	7.90
50	5.71
55	4.30
60	3.31
65	2.61
70	2.09
75	1.68
80	1.38
85	1.15
90	1.0
95	.897
100	.832
105	.799
110	.777
115	.762
120	.758
125	.760
130	.776
135	.805
140	.851
145	.911
150	.995
155	1.11
160	1.27
165	1.49
170	1.79
175	1.88
180	1.97

* Data adapted from measurements taken in the channel between Catalina Island and the California coast. Reprinted in "Volume Scattering Functions for Selected Ocean Waters," Theodore J. Petzold, Scripps Institution of Oceanography Report SIO Ref. 72-78, October 1972.